REPORT DOCUMENTATION PAGE

Form Approved
OMB NO. 0704-0188

1. AGENCY USE ONLY (Leave Blank)	2. REPORT DATE	3. REPORT TYPE AND DATES COVERED
	2/20/2003	FINAL REPORT, 08-JUL-02 TO 07-JAN-03

4. TITLE AND SUBTITLE
Identification of Magnetic Materials By Discrete Fourier Analysis

5. FUNDING NUMBERS
DAAD19-02-I-0293

6. AUTHOR(S)
Martha Pardavi-Horvath

7. PERFORMING ORGANIZATION NAME(S) AND ADDRESS(ES)
The George Washington University
801 22nd Street, NW Washington, D.C. 20052

8. PERFORMING ORGANIZATION REPORT NUMBER

9. SPONSORING / MONITORING AGENCY NAME(S) AND ADDRESS(ES)
U. S. Army Research Office
P.O. Box 12211
Research Triangle Park, NC 27709-2211

10. SPONSORING / MONITORING AGENCY REPORT NUMBER
43802-MS-II

11. SUPPLEMENTARY NOTES
The views, opinions and/or findings contained in this report are those of the author(s) and should not be construed as an official Department of the Army position, policy or decision, unless so designated by other documentation.

12 a. DISTRIBUTION / AVAILABILITY STATEMENT
Approved for public release; distribution unlimited.

12 b. DISTRIBUTION CODE

13. ABSTRACT (Maximum 200 words)

A novel approach, linking microstructural effects, magnetic measurements, and signal processing methods, was developed to analyze, identify and compare magnetic materials. The Discrete Fourier Transform (DFT) was applied to DC remanent magnetization curves (RHL) and to Switching Field Distribution (SFD). It was shown analytically how the a_n, b_n Fourier coefficients depend on the width of SFD, on the coercivity, and on the highest applied field. The field and the coercivity dependences can be separated by using complex Fourier coefficients.

The effects of magnetic and sampling parameters on the DFT were numerically simulated. Based on the results of the analytical and numerical study, a measurement and DFT protocol was developed to analyze magnetic materials. The sensitivity of DFT to magnetic markers was investigated numerically, by varying the matrix/marker ratio and the relative coercivities. The measurement and FFT protocol was applied to commercial magnetic media (DELTACARD, METROCARD) and Fe-Zn nanocomposites.

The results are submitted to two international conferences. Participation in this complex research gave a significant contribution to the education of two graduate and one undergraduate students..

14. SUBJECT TERMS	15. NUMBER OF PAGES
magnetic hysteresis, FFT, DFT, coercivity, remanence, magnetic measurement	51
	16. PRICE CODE

17. SECURITY CLASSIFICATION OR REPORT	18. SECURITY CLASSIFICATION ON THIS PAGE	19. SECURITY CLASSIFICATION OF ABSTRACT	20. LIMITATION OF ABSTRACT
UNCLASSIFIED	**UNCLASSIFIED**	**UNCLASSIFIED**	**UL**

REPORT DOCUMENTATION PAGE (SF298)
(Continuation Sheet)

IDENTIFICATION OF MAGNETIC MATERIALS BY DISCRETE FOURIER ANALYSIS

M. Pardavi-Horvath
Department of Electrical Computer and Engineering
The George Washington University, Washington, DC 20052, USA
mpardavi@gwu.edu

OUTLINE

1. INTRODUCTION

1.1. Motivation and objectives

Magnetic materials are extensively used in high technology, first of all, in information storage on tapes, disks, and magnetooptical media. Magnetic markers are used for fraud and theft prevention, identification, as in security tags, bank checks, and as currency markers. Most of the applications are based on particulate magnetic materials. For example, in traditional recording media, credit cards, key cards, or as thin film recording media with decoupled grains. Magnetic nanocomposites of small magnetic particles, embedded in a nonmagnetic matrix, are in focus of investigations for application in high density recording, pigments, absorbing microwave coatings, ferrofluids, magnetic refrigeration, etc.

Depending on the actual application, different range of particle size (multidomain, single-domain, superparamagnetic) is preferred. Some application requires high size uniformity (narrow linewidth in microwave materials, broad linewidth in EMI absorbers). Although the magnetic properties are specified for a given application, even slight changes in the technological process can lead to significant magnetic changes, related to microstructural variations. Due to the unique sensitivity of the magnetic properties to shape and size of the constituting particles, it is desirable to characterize the magnetic (in)homogeneity of these materials by quick, reliable and inexpensive methods. X-ray diffraction, Mossbauer spectroscopy, Scanning Transmission Electron Microscopy (STEM) are the raditional, sophisticated, and important tools for this purpose, but they are neither simple, nor inexpensive methods. Frequently, a faster, but possibly less accurate method of characterization of separate magnetic fractions would be sufficient, in order to give a feedback to the technological process. The question of quantitative *magnetic* characterization of non-magnetic properties, like the distribution of shape and size, homogeneity and uniformity, still remains open.

It was proposed to study of Discrete Fourier Analysis of the DC remanence curves (RHL) and the irreversible susceptibility (SFD), as a quick and inexpensive tool for characterizing the switching field distribution. It is assumed that it is directly related to the microstructural peculiarities of the material, the size, shape, and interaction distribution of the constituting particles, i.e. magnetic identity of magnetic materials.

In signal processing it was wellknown for a long time that the transformation of a signal from time-domain into the frequency domain can give much more information about the details of the signal than the original signal itself. The Fourier transformation is a standard tool in electrical engineering. One of the greatest achievements of numerical analysis during the past decades is the establishment of the theory of discrete Fourier transforms (DFT). One application of the DFT, - the Fast Fourier Transform (FFT) - is a routine process in signal processing, spectroscopy, curve fitting, noise reduction. Software FFT modules are widely available, they are user friendly and inexpensive. The Fourier transform is a unique fingerprint of the given magnetic material, - this fact is proposed for magnetic marking and identification purposes.

The proposed research was a natural outgrowth of an ongoing experimental investigation of the properties of magnetic nanocomposites. Our original efforts were directed toward finding a quick and simple method to characterize the (in)homogeneity of magnetic nanocomposites, prepared by reaction milling, and to follow the microstructural and magnetic changes during the technological process [1-3].

It was proposed to use the Discrete Fourier Transform (DFT) of the hysteresis loop to *describe, characterize, compare, and identify magnetic materials*, based on the statistical properties of the particle distribution, reflected in the DFT of the hysteresis loop. Because of the tremendous increase in speed, the FFT could be a routine tool to analyze, and/or identify magnetic materials.

During the research, supported by the ARO grant, the followings tasks were completed:

- The relationship of the classical Fourier Transform and the Discrete Fourier Transform (DFT) was analyzed with special emphasis on amplitude and phase relationships;
- The analytical relationship between the Fourier spectrum and the magnetic hysteresis, the major loop, the major remanent hysteresis loop (RHL), and the derivative of the RHL, i.e. the Switching Field Distribution (SFD) curve was analyzed;
- Different numerical distributions, corresponding to different RHL, and sums of overlapping

distributions, using the error function for RHL and Gaussian distribution function for SFD were numerically simulated to assist the understanding of the FFT representation. The models correspond to real composite and multiphase materials. Both amplitude and phase information was used to identify material properties; based on the results of simulation, a protocol of measuring hysteresis loops and performing the Fourier transforms was developed;

- The proposed FFT analysis was applied to several classes of commercial magnetic materials by measuring the hysteresis loops on a Vibrating Sample Magnetometer, generating SFD curves by numerical differentiation; and applying MATLAB's FFT routine to the RHL and SFD curves.
- Conclusions about the applicability of commercial FFT routines to characterize magnetic materials, and proposed further research directions were outlined.

1.2. Magnetic hysteresis

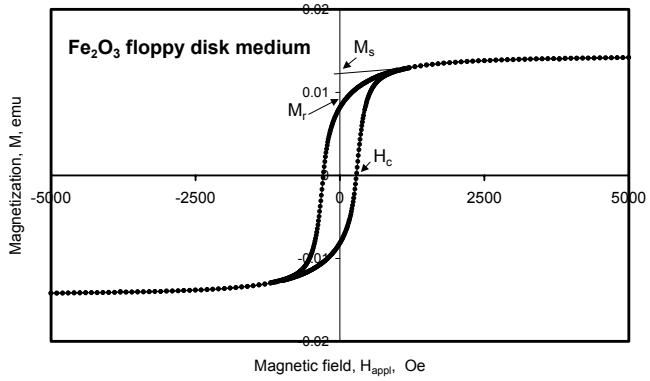

Fig. 1.1 Major hysteresis loop of a floppy disk sample. M_s - saturation magnetization, M_r - remanent magnetization, H_c - coercivity.

The industrial technology of preparation of commonly used magnetic materials enables different manufacturers to produce large quantities of the raw magnetic material with very similar basic magnetic characteristics. Magnetic materials are routinely characterized by their ***hysteretic*** behavior, i.e. the dependence of the magnetization on externally applied magnetic field, M vs. H_{appl}, as illustrated in *Fig.1.1*. The hysteresis loop can be conveniently measured by a wide range of commercially available magnetometers. Saturation magnetization (M_s), coercivity (H_c), and remanence (M_r) are the main characteristics, obtained from the *major hysteresis loop* (MHL) measurements. However, the magnetic hysteresis loop provides ***average*** information, i.e. the mean values for the sample under test, which contains a large number of particles, or switching units. As in the case of any object, consisting of a large number of elements, it should be treated as a statistical ensemble. The upper and lower limits of the given property, i.e. width of the distribution, determines the critical behavior, stability, and fault tolerance of the system.

Therefore, the knowledge of the statistical distribution of properties is very important for the reliability of the system in application. Unfortunately, the hysteresis loop is not sensitive to the statistical distribution of the properties of the particles of the material. It is possible to reproduce magnetic materials with the same M_s, H_c, and M_r, and still having significantly distinct statistical distribution of shapes, sizes, defects, and interactions between the constituting elements of the sample under test, i.e. its *microstructure*. The statistical distribution is what makes a material unique. To measure and reproduce the mean magnetic parameters of a material, is relatively easy. At the same time, it is very hard to reproduce the microstructure and the statistical distribution of particles. This is the basis for "fingerprinting" a magnetic material. The major hysteresis loop carries only very limitedinformation about the statistical nature of the given magnetic material.

The hysteresis loop is composed of a sequence of individual events of switching of the particles of a bulk sample. Each particle, or switching unit has a different switching field. These switching fields follow a certain statistical distribution. The mean value of the switching fields is the coercivity, H_c. The derivative of the major hysteresis loops $\chi = dM/dH$, can be used to get information about the distribution of particle switching properties. The magnetization, obtained at a given value of the field, represents the contribution of the particles to the magnetization that have switched into the field direction. The field dependence of the magnetization thus is expected to reflect the distribution of particles, i.e. the derivative is related to the *switching field distribution* (SFD).

The problem is, that the switching field distribution, as given by the *dM/dH* curve, is a function of several

factors. It contains the distribution: 1. the individual switching fields of individual particles, caused by the defect structure, compositional, shape and size variations; 2. the reversible contributions to the magnetization process, and 3. the distribution of the magnetostatic interaction fields with other particles. It is not easy to separate these contributions, although several theoretical attempts have been made to identify them in the frame of the Preisach models of magnetic hysteresis [4].

Moreover, the hysteresis loop is shape dependent, due to the shape demagnetizing factors, N, leading to a demagnetizing field, $\boldsymbol{H_D} = -N\boldsymbol{M}$. The state of the magnetization of the material corresponds to the *internal field*, experienced by the sample under test (SUT), and the internal field is a strong function of the shape of the sample

$$\boldsymbol{H_{int}} = \boldsymbol{H_{appl}} - N\boldsymbol{M}$$

To illustrate the role of the shape, let's look at the coercivity for a long wire of a soft magnetic material, magnetized along the wire axis. In this case, H_c is negligible, and saturation is reached in a very small field, i.e. the hysteresis loop is practically rectangular, and its derivative has a very sharp peak. On the other hand, when the *same wire* is magnetized across its diameter, it takes a field of $H_{appl}=H_D=2\pi M_s$ to counteract the demagnetizing field, and to reach the internal field, necessary for saturation. In this case the derivative, i.e. the SFD has a broad flat shape, for the same piece of the same material. Evidently, here the usual definition of the SFD fails, as the results of the measurements depend on the shape of the SUT.

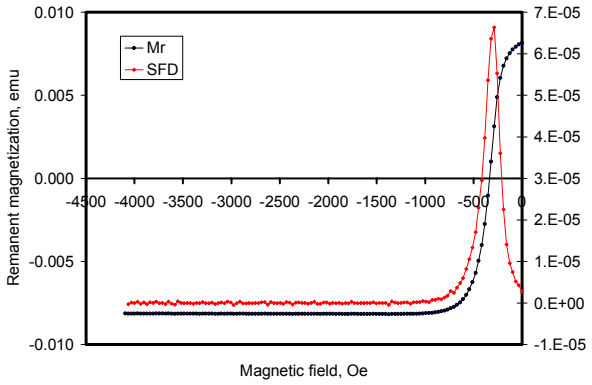

Fig. 1.2 DC remanent hysteresis loop (RHL) and switching field Distribution (SFD) for a floppy disk recording medium of *Fig.1.1.*

To avoid the shape dependence, we've proposed to use the ***DC Remanent Hysteresis Loop*** (RHL) and its derivative (SFD) to obtain information about the switching field distribution [3]. The remanence, obtained at a given value of the field, represents the contribution of the particles to the magnetization that have *irreversibly* switched into the field direction. The RHL measurement mode is offered for all commercially available magnetometers. The measurement of the RHL starts with a large positive saturating field, decreased to $H = 0$, and then the *remanent magnetization*, M_r, is measured after reducing $H = 0$; then the field is lowered to $-H_i$, with subsequent return to $H = 0$, and the remanent magnetization, M_{ri}, is measured again in $H = 0$. The sequence of M_r vs. $-H$ is called the RHL. In the following, the derivative of the RHL it denoted as SFD. *Fig.1.2* illustrates the RHL and SFD for a commercial 5" Co doped γ-Fe_2O_3 floppy disk.

Based on these observations, it was proposed that instead of the major hysteresis loop to use the DC Remanent Hysteresis Loop (RHL) to characterize the material, and to characterize the switching field distribution (SFD), as a measure of the statistical distribution of the particles.

1.3. Previous related research

Hysteresis is a multivalued, nonlinear function, and for many years a tremendous effort was devoted to numerical modeling of hysteresis curves. One approach was to construct a hysteresis loop from a series of exponentials, from where it was a direct route to describe *B(H)* and *M(H)* curves by their Fourier components. Application of the Fourier transformation technique to magnetic hysteresis was proposed by several authors, as early as 1971 [5]. It was shown that the Fourier transform of the major hysteresis loop can be used to characterize magnetic materials [6-18].

In some previous works the Preisach model of magnetic hysteresis and the Fourier description was combined [19-20]. All the previous authors used the classical Fourier transform (FT) of the measured major hysteresis loop. Due to the inherent limitations of the classical FT, the loops should be made symmetrical and folded in order to have a periodic function before performing the FT. But this is only an inconvenience, compared to the real problem that the major loop contains information about the reversible part of the

magnetization and the sample shape, which would be very hard to identify in terms of the properties of the constituting particles. The previous authors came to the conclusion that the Fourier transform is characteristic of a given material, and a few components adequately describe the hysteresis loop. There was no effort to analyze the underlying physics and link the magnitude and phase of the Fourier components in the frequency domain to the composition of the material.

From the time of the previous efforts to use the Fourier transform of the hysteresis loop, the discrete, fast FT (FFT) became an integral part of many commercial software packages [21-27], therefore it was proposed by this P.I. to use the FFT of the SFD to *describe, characterize, compare, and identify magnetic materials*, based on the statistical properties of the particle distribution, reflected in the FFT of the SFD. In this case there is no need to periodicize the hysteresis loop, the FFT can be directly applied to the SFD curves. Because of the tremendous increase in speed, the FFT could be a routine tool to analyze, and/or identify magnetic materials.

The "magnetic" FFT could be analyzed based on the following considerations. Assume a function f(H_k) of field, measured at discrete values H_k. In our case we identify the *M(H)* dependence with this function, as *H* is changed over time *H(t)*. Introducing the reciprocal μ space with $\mu_p=2\pi p/H$, where p = 0,1,2,...2N-1, we may construct

$$F(\mu_p) = \frac{1}{2N}\sum_{k=0}^{2N-1} f(H_k)\exp(iu_p H_k), \quad \text{and} \quad F(H_k) = \sum_{k=0}^{2N-1} F(\mu_p)\exp(-iu_p H_k).$$

These functions are the discrete Fourier transform pair. Taken as a pair of mathematical relations it is exact, and these equations, defining 2N component vectors, become matrix equations, what can be solved by usual numerical methods. The inverse space, i.e. *1/H* can be associated with $\mu = (1/M_{r0})\,(dM_r/dH)$, i.e. directly related to the SFD.

The limitations of the discrete FT arise when we try to apply it to real physical systems and attempt a physical interpretation and generalization of $F(\mu_p)$ to a continuous $F(\mu)$. However, all real measurements are discrete series of data, and the DFT is, in fact, a natural tool to analyze the measured magnetization curves. To perform a numerical FT, the early FFT routines required that measurements should be done at equidistant field intervals, and the number of measurement points N should be an integer power of 2. The latest FFT modules (MATLAB, ORIGIN, TABLECURVE) do not require equidistant measurement points, they perform the interpolation, and if the number of the data points is not a power of 2, or not a prime, the datasets can be padded with zeros. One important precaution is to take, that any component of higher angular frequency than $\mu_N = 2\pi N/H$ should be excluded. In fact, this is why the FFT is a powerful noise reduction tool in signal processing. Any commercial FFT software, available for signal analysis, can be used for separating overlapping distribution functions by FFT editing the frequency domain spectra - exactly what we need for characterization of multi-component materials.

Our results prove that the FFT spectra are very sensitive to even very slight changes in material properties, but one has to be careful with the interpretation. The interpretation of the results is, in fact, not a simple task. Indeed, it is sometimes contra-intuitive, as could be seen from the earlier Fourier analysis attempts. For example, a narrow statistical distribution corresponds to a broad FFT spectrum, i.e. a very large number of Fourier components (in the limit of a square loop, the number of components is infinite), or for a very broad distribution of properties, the Fourier spectrum is narrow. For overlapping distributions of composites or multiphase materials, having different mean values and widths, the assignment of spectral lines is not straightforward, and special care should be made to follow the same measurement and evaluation protocol for the samples to be compared, as it was developed during this research and illustrated in the following sections.

2. The Fourier Transform (FT) and the Discrete Fourier Transform (DFT)

2.1. Fourier Transform (FT)

The *Fourier Transform*, in essence, decomposes or separates a waveform or function into sinusoids of different frequency which sums to the original waveform.

FT is a generalization of the complex Fourier series in the limit as period $L \to \infty$.

$$f(x) = \int_{-\infty}^{\infty} F(k) e^{2\pi jkx}\, dk \tag{2-1}$$

$$F(k) = \frac{1}{2\pi} \int_{-\infty}^{\infty} f(x) e^{-2\pi jkx}\, dx \tag{2-2}$$

Here,

$$F(k) = \mathcal{F}_x[f(x)](k) = \int_{-\infty}^{\infty} f(x) e^{-2\pi jkx}\, dx \tag{2-3}$$

is called the *forward* Fourier transform, and

$$f(x) = \mathcal{F}_k^{-1}[F(k)](x) = \frac{1}{2\pi} \int_{-\infty}^{\infty} F(k) e^{2\pi jkx}\, dk \tag{2-4}$$

is called the *inverse* Fourier transform.

2.2. Discrete Fourier Transform (DFT)

Because of digital computers which only work with finite number of discrete data points, computation of the FT of a data set, requires a technique which is widely known, called *Discrete Fourier Transform (DFT)*. DFT gives N (equally spaced) discrete frequencies for N data samples, $x(n)$ is values of samples in time domain and $X(k)$ is values of samples in frequency domain.

DFT $$X(k) = \sum_{n=0}^{N-1} x(n) e^{-j2\pi kn/N} \tag{2-5}$$

IDFT $$x(n) = \frac{1}{N} \sum_{k=0}^{N-1} X(k) e^{j2\pi kn/N} \tag{2-6}$$

where IDFT is *Inverse DFT*, which brings back the values from frequency domain to time domain.

2.3. Fast Fourier Transform (FFT)

The Fast Fourier transforms (FFT) are efficient and fast discrete Fourier transform (DFT) algorithms which reduce the number of computations needed for N points from $2N^2$ to $2N \lg N$, where lg is the base-2 logarithm.

If the function to be transformed is not harmonically related to the sampling frequency, the response of an FFT looks like a sinc function (although the integrated power is still correct).

Fast Fourier transform algorithms generally fall into two classes: decimation in time, and decimation in frequency. The Cooley-Tukey FFT algorithm first rearranges the input elements in bit-reversed order, and then builds the output transform (decimation in time). The Danielson-Lanczos method breaks the DFT into two parts, based on the number of points as an integer power of 2. The basic idea is to break up a transform of length *N* into two transforms of length *N/2*. Commercial algorithms (MATLAB, ORIGIN, TABLECURVE, etc) are using different FFT routines, based on different approach of dealing with arbitrary numbers. Although the FFT of a function, or signal, is expected to be the same, this is not always the case. Frequently, the differences are due to the different graphical representation. It is suggested to use the same FFT algorithm to compare the DFT series of the materials under test. In this work MATLAB's FFT algorithm was used, and compared to DFT data, obtained from ORIGIN PRO7.

2.4. Definitions used

In this work we apply the well-known technique of FFT to derive more information from the measured *M-H* hysteresis loops and its derivative, the switching field distribution (SFD). As a model, the *erf* function is used to represent the remanent hysteresis loops (RHL) and the *Gaussian* function for SFD.

$$\mathrm{erf}(x) = \frac{2}{\sqrt{\pi}} \int_0^x e^{-\alpha^2} d\alpha \qquad (2\text{-}7)$$

$$f(x;\mu,\sigma) = \frac{1}{\sqrt{2\pi\sigma}} e^{-\left(\frac{(x-\mu)^2}{2\sigma^2}\right)} \qquad (2\text{-}8)$$

where μ is the arithmetic mean of the Gaussian distribution, which represents H_c (coercivity), and σ is the standard deviation of the distribution, corresponding to SFD width.

The relationship between the integral of the gaussian Eq.(2-8) and the error function Eq.(2-7) is as follows:

$$F(x;\mu,\sigma) = \mathrm{erf}\left(\frac{x-\mu}{\sqrt{2\sigma^2}}\right) \qquad (2\text{-}9)$$

In the following, analytical and numerical calculations performed in this research will be described to show the sensitivity of different parameters of *M-H* loop with their harmonics.

3. FOURIER TRANSFORM (FT) AND DISCRETE FOURIER TRANSFORM (DFT) OF MAGNETIC HYSTERESIS

3.1. Linear model of the M-H loop

In a previous work on harmonic analysis of *M-H* loops it was shown on a simplified linear model how each harmonics will behave if we represent the *M-H* loops with linear segments [6]. This model assumes that the *M-H* loop can be represented with straight lines, as a time function in a way that starting from H=0 at t=0 and the field is increased in time up to the maximum value $+H_{max}$, then down to $-H_{max}$, till it makes a complete hysteresis loop during a full period, at $t=T$.

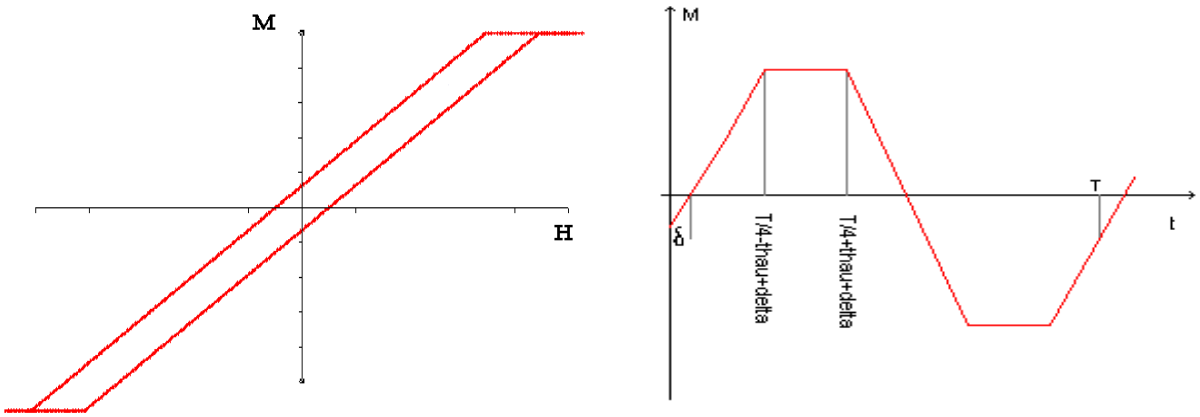

Fig.3-1 (a) M-H loop for non- zero coercivity model, (b) time domain representation of M(t)

The authors of [6] developed the sine and cosine series representation for the waveform, shown in the Fig.3-1(b) with coercivity (H_c) either equal zero, or a finite H_c =δ.

The standard Fourier series gives

$$a_n = \frac{2}{T}\int_0^T B(t)\cos\left(\frac{2\pi nt}{T}\right)dt \qquad (3-1)$$

$$b_n = \frac{2}{T}\int_0^T B(t)\sin\left(\frac{2\pi nt}{T}\right)dt \qquad (3-2)$$

and the results of simulation for H_c=0 in [6] were given as

a_n=0, for all n (3-3)

b_n=0, for even n (3-4)

$$b_n = \frac{8a}{T}\left(\frac{T}{2\pi n}\right)^2 (-1)^{(n-1)/2}\cos\left(\frac{2\pi n\tau}{T}\right) \quad \text{for odd n.} \qquad (3-5)$$

where "*a*" was defined as the gradient of the curve below saturation, i.e. $a=dM/dt$, and τ is the time spent at saturation, corresponding to the maximum applied magnetic field above the saturation field, $\tau = H_{max}-H_{sat.}$ The results of simulation for $H_c \neq 0$ in [6] were

a_n=0, for n even (3-6)

$b_n=0$ for n even (3-7)

$$a_n = -\frac{8a}{T}\left(\frac{T}{2\pi n}\right)^2 (-1)^{(n-1)/2}\cos\left(\frac{2\pi n\tau}{T}\right)\sin\left(\frac{2\pi n\delta}{T}\right) \quad (3\text{-}8)$$

$$b_n = \frac{8a}{T}\left(\frac{T}{2\pi n}\right)^2 (-1)^{(n-1)/2}\cos\left(\frac{2\pi n\tau}{T}\right)\cos\left(\frac{2\pi n\delta}{T}\right) \quad (3\text{-}9)$$

for odd n.

As it can be seen, both Fourier coefficients, a_n and b_n, are dependent both on the coercivity δ and the time spent in saturation (τ), i.e. the maximum applied field above saturation.

In this part the results of [6] are extended and revisited with another approach. Instead of expanding *M(t)* into the Fourier series of sine and cosine waves, here the complex form has been used.

$$C_n = \frac{1}{T}\int_0^T M(t)\, e^{-j2\pi nt/T} \quad (3\text{-}10)$$

where *T* is the time period of the flux wave, *M(t)* is magnetization in time.varying according to the following formulas:

$$M(t)=\begin{cases} t-\delta & 0\le t\le \frac{T}{4}-\tau+\delta \\ 1(\frac{T}{4}-\tau) & \frac{T}{4}-\tau+\delta\le t\le \frac{T}{4}+\tau+\delta \\ (\frac{T}{2}+\delta)-t & \frac{T}{4}+\tau+\delta\le t\le \frac{3T}{4}-\tau+\delta \\ -1(\frac{T}{4}-\tau) & \frac{3T}{4}-\tau+\delta\le t\le \frac{3T}{4}+\tau+\delta \\ t-(T+\delta) & \frac{3T}{4}+\tau+\delta\le t\le T \end{cases} \quad (3\text{-}11)$$

where δ is the coercivity, Substitution into Eq.(3-10) gives:

$C_n= 0$ for even n (3-12)

$$|C_n| = 4(\alpha\sin(\frac{2\pi n\tau}{T}) + \beta\cos(\frac{2\pi n\tau}{T})) \quad (3\text{-}13)$$

where

$$\alpha = \frac{T}{4\pi^2 n^2} \quad \text{and} \quad \beta = \frac{\frac{T}{8}-\frac{\tau}{2}-\frac{1}{2}}{n\pi}$$

$$\angle C_n = \frac{n\pi(T+2\delta)+T\pi}{2T} \quad (3\text{-}14)$$

for all odd n

As it can be seen from Eq.(3-13) C_n does not depend on changes in coercivity (δ), however it reflects changes in τ. In contrast, the phase contains the coercivity changes, but it does not depend on τ (or the time spent in saturation). The following figure is simulation of this calculation with MATLAB.

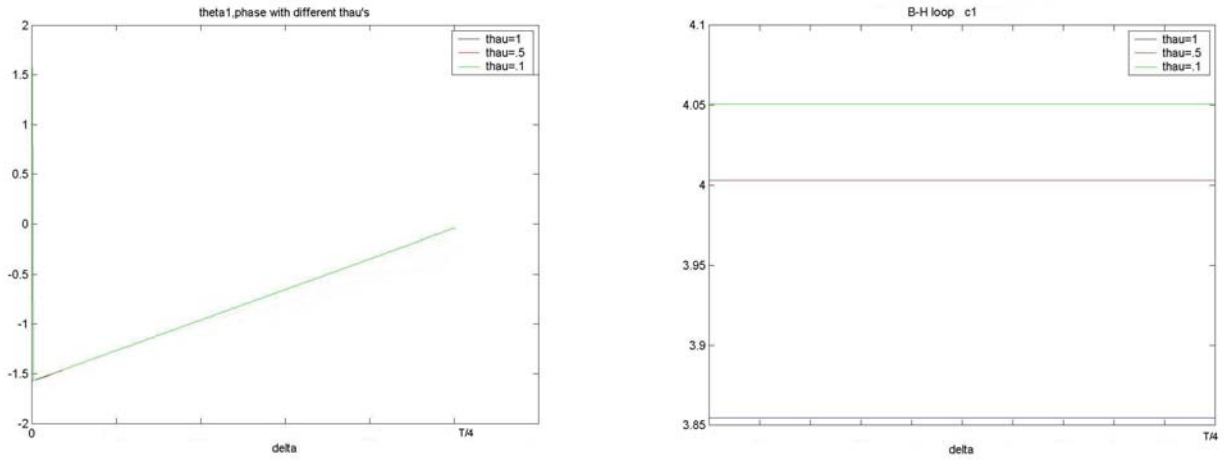

Fig.3-2 (a) Phase of the first harmonics vs. δ. (b) Amplitude of the first harmonic vs. δ (coercivity) for different values of τ (H_{max})

In the analytical sine-cosine series, both Fourier components depend on both the coercivity and on the maximum magnetic field above the saturation, while, as it was shown here, using the exponential form the two effects are separated, and can be studied independently.

3.2. Non-linear (erf function) model

In order to be able to predict the behavior of the harmonics of the *M-H* loop in more realistic way, a model of the loop by an error function was developed. The Fourier series coefficients were evaluated for this model. The *erf*, a cumulative Gaussian distribution is a good approximation for the behavior of the DC remanent hysteresis loop.

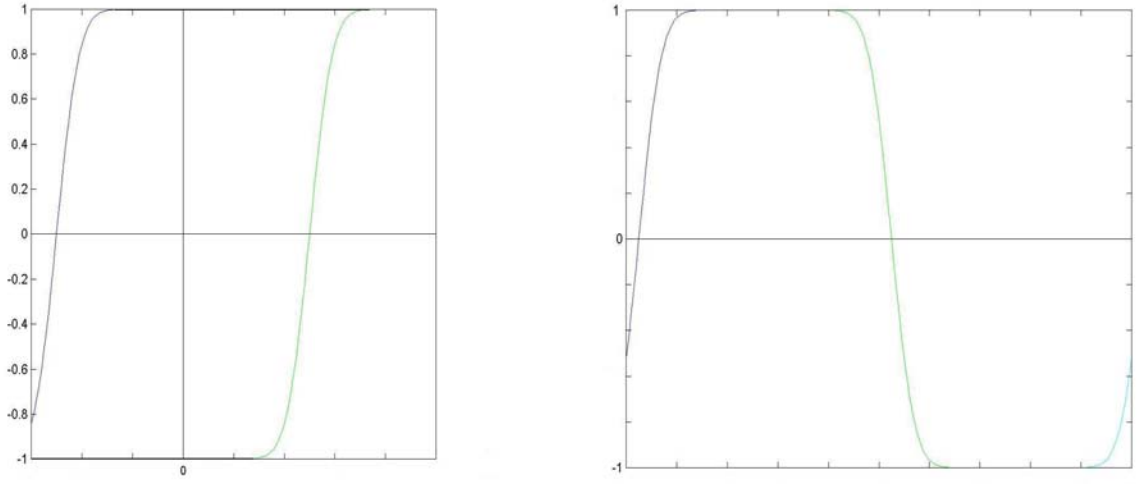

Fig. 3-3 (a) The *erf* function model of the RHL hysteresis loop; (b) Time domain representation of the non-linear model of the *M-H* loop using the error function

This model includes all the parameters of a real *M-H* loop (H_c, H_{max}, δ, τ) and we can have numerical control on each and every of them.

$$M(t)=\begin{cases}\operatorname{erf}\left(\dfrac{t-\delta}{\sqrt{2\sigma^2}}\right) & 0\le t\le \dfrac{T}{4}-\tau+\delta \\ 1 & \dfrac{T}{4}-\tau+\delta\le t\le \dfrac{T}{4}+\tau+\delta \\ \operatorname{erf}\left(\dfrac{(\frac{T}{2}+\delta)-t}{\sqrt{2\sigma^2}}\right) & \dfrac{T}{4}+\tau+\delta\le t\le \dfrac{3T}{4}-\tau+\delta \\ -1 & \dfrac{3T}{4}-\tau+\delta\le t\le \dfrac{3T}{4}+\tau+\delta \\ \operatorname{erf}\left(\dfrac{t-(T+\delta)}{\sqrt{2\sigma^2}}\right) & \dfrac{3T}{4}+\tau+\delta\le t\le T \end{cases} \qquad (3\text{-}15)$$

The only assumption in this model is that we are in the saturation region far enough that we can assume that within above ranges for the second and fourth terms the error function in Eq. 3-15 reaches 1 and –1 respectively. The model was evaluated numerically, due to the lack of simple analytical integrals for the modified *erf*. Figure (3-3-b) shows an *M-H* loop, represented by *erf* in such a way that it is unfolded in time and it shows a complete closed loop from $-H_{max}$ to $+H_{max}$, which is defined as period *T* of the M-H loop in time domain.

The linear model of [6] gave a very good illustration of the FT of a simple model hysteresis loop. The *erf* model, introduced here in Eq. 3-16, is more realistic. In the following, this realistic model will be compared to the linear model, which was introduced earlier, and with the sine-cos linear model in [6]. So, first this model is expanded into sine and cosine waves, according to Eq. (3-1) and Eq. (3-2), while *erf* is defined by Eq. (2-7). The Fourier coefficients can be found by substituting Eq. (2-7) into Eq. (3-15) and then applying Eq. (3-1) and Eq. (3-2). However, there is no simple analytical solution for these integrals. Therefore, the integrals Eq. (3-1) and Eq. (3-2) were solved numerically with MATLAB.

Amazingly, we find that the linear model is a very good approximation for the *M-H* loop. Fig. (3-5) illustrates the dependence of the first coefficients on the coercivity for different maximum applied magnetic field, for the case of the standard deviation of σ^2=0.5, which are very close to the results in [6]. In these Figs the coercivity is given in units of *T*.

As it can be seen from Figs. (3-5) the Fourier coefficients depend very strongly on the coercivity and on the maximum applied field during the measurement of the hysteresis loop.

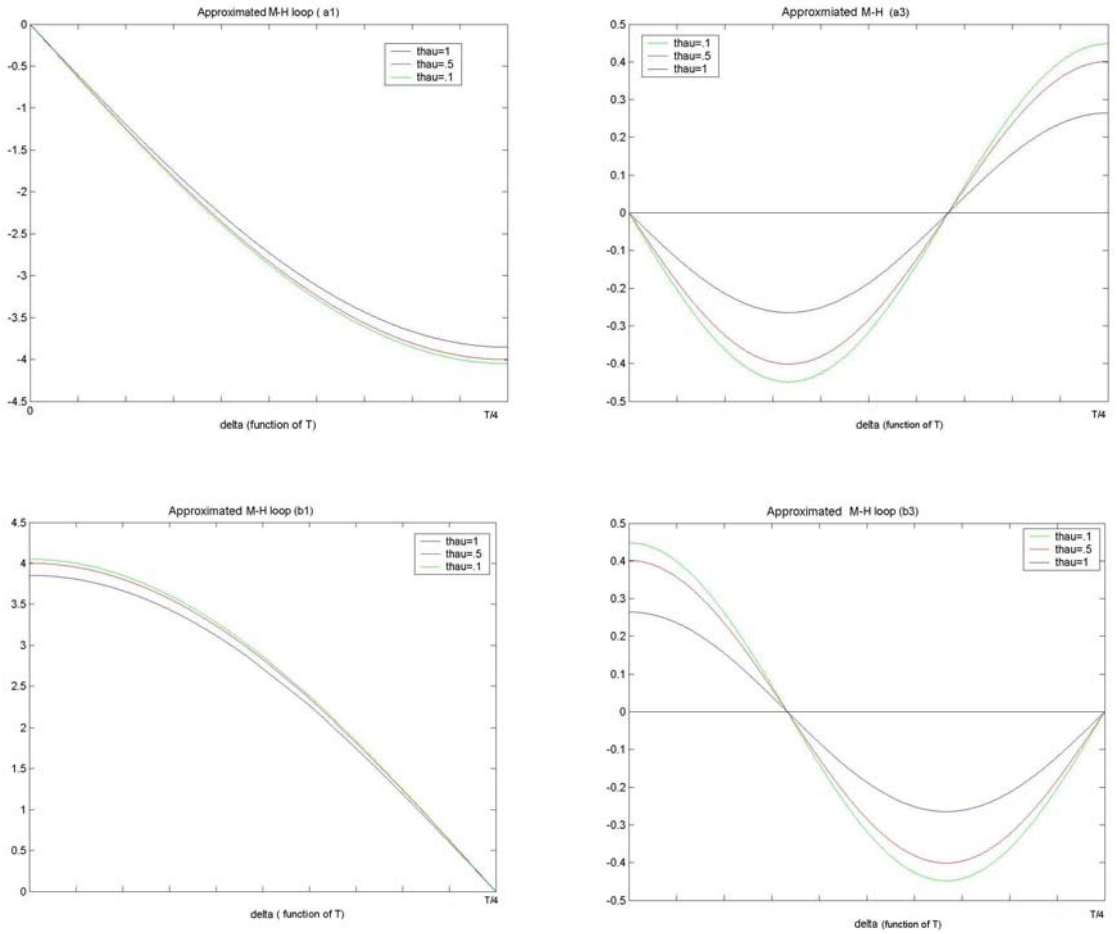

Fig.3-5 The *erf* model of the M-H loop: the amplitude of first *sine-cos* coefficients a_1, a_3 (first row), and b_1, b_3 (second row) vs. coercivity δ (given in terms of *T)*, for different values of τ.

And, as it was expected, when converting to the complex coefficients, the two effects are separated, the complex coefficients do not depend on the coercivity, H_c shows up in the phases.

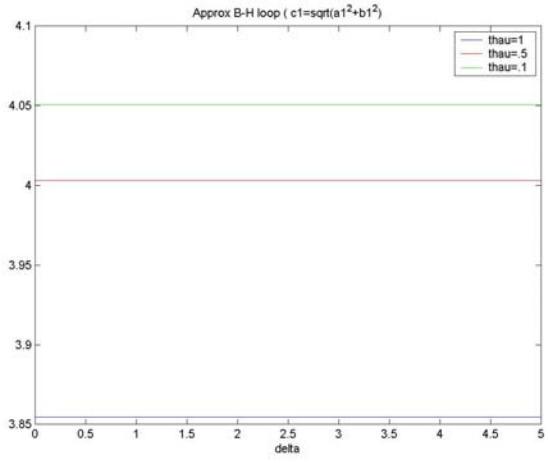

Fig.3-6 The *erf* model of *M-H* loop: C_1 complex amplitude of the first harmonic vs. coercivity δ for different values of τ.

The model was evaluated for more realistic values of coercivity δ and σ. For the simulation shown in Fig. 3.7. it was assumed that the maximum applied field is H_{max} =6H_c, and saturation is reached at different fields,

i.e. for different values of parameter τ. The later assumption corresponds to the physical picture of different width of the Gaussian distribution of the switching fields.

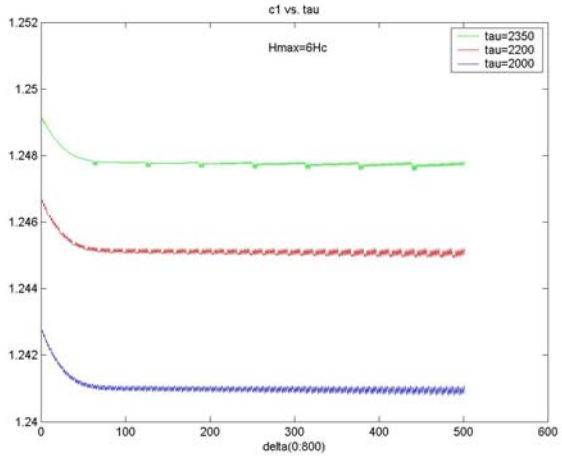

Fig. 3-7 Coercivity (δ) dependence of the C_1 coefficient of the FT of *erf* for H_{max}=6 H_c, for different values of time spent in saturation τ.

As it can be seen from Figure 3.7, the C1 coefficients slightly depend on τ, and it takes some time to converge to a constant value. The ripples are numerical artifacts. So with realistic values still it can be concluded that the complex coefficients of Fourier series are independent of coercivity.

3.3. Conclusion

In this part of the research, an analytical model was developed to represent the DC remanent magnetic *M-H* hysteresis loops, based on the *erf* function. It was shown that the a_n, b_n coefficients of the FT depend on the width of the switching field distribution through the standard deviation of the Gaussian, - underlying the *erf* -, both depend on the coercivity, represented by δ, and τ, the time spent in saturation. The field and coercivity dependencies can be separated by using complex Fourier coefficients, where the absolute value just depends on τ, and the phase depends on coercivity. An interesting result is that the Fourier coefficients strongly depend on the maximum applied field, above the saturating field, i.e. the total period *T* of the curve. This is reasonable, assuming the existence of the "*paraprocess*", i.e. the continuation of the alignment of the magnetization with the field up to fields much above saturation. The simple linear model also contains this result.

These analytical results are the foundation to be able to analyze the DFT results, obtained by numerical FFT algorithms, and to recommend a measurement and evaluation protocol for analysis and comparison of the FFT of the RHL.

4. NUMERICAL MODEL AND DEVELOPMENT OF AN FFT PROTOCOL FOR CHARACTERIZING MAGNETIC MATERIALS

4.1. Numerical model

Several simplifying assumptions were made in numerical simulation of the magnetic hysteresis. The numerical models of the SFD are based on the Gaussian distribution G of the particles in the magnetic materials, and on the integral of the Gaussian, the error function, *erf,* as the model for the RHL. Although the hysteresis loop is a strongly nonlinear, multivalued function of the magnetic field, this approach is not far from the reality, where the distribution of the particles properties in particulate magnetic materials can be assumed independent, following a normal distribution.

As the hysteresis loop is a symmetric function of the magnetic field, we consider only a part of it for analysis (i.e. the part which can be considered to be in the second quadrant of the coordinate axes).

The error function, corresponding to the RHL is defined by the formula

$$erf = \frac{1}{\sigma\sqrt{2\pi}} \int_{-\infty}^{x} e^{-\frac{(x-\mu)^2}{2\sigma^2}} dx \qquad (4.1)$$

where σ is the standard deviation; and μ is the mean value of the function ;

When applied to the RHL, σ corresponds to the halfwidth of the switching field distribution (SFD) curve, and x in the error function is analogous to the applied magnetic field H, with μ is the mean value being the coercivity (H_c).

The derivative of the error function results in a Gaussian function. The derivative of M_r with respect to H is dM_r/dH, which is nothing but the switching field distribution SFD when plotted against H.

The Gaussian function can be defined as

$$G(x) = \frac{1}{\sigma\sqrt{2\pi}} e^{\frac{-(x-\mu)^2}{2\sigma^2}} dx \qquad (4.2)$$

4.2. The effect of the model parameters on the FFT

In order to assess the influence of different material parameters on the FFT, the main parameters of the model (σ, μ, x and the number of points in the function) were systematically changed, and the resulting FFT curves were analyzed. The various parameters in the error function and Gaussian are changed one at a time keeping the rest constant. This enables in giving a clear picture of the effect of each parameter on the FFT.

The experiments are done on MATLAB. The *normcdf* and *nornpdf* functions are used to represent the error function and Gaussian respectively.

Four basic numerical experiments are performed to study the effect of change in material parameters: σ (the width of the distribution,) and μ (the coercivity, mean), and the sampling parameters :the number of the "measured" points in the functions, and the magnetic field limits (period, T).

4.2.1. Effect of varying the standard deviation

To analyze the effect of different statistical distribution of the particles in different materials, the width of the property distribution was changed by changing the σ. Three simulations were performed. The results of two of the simulations are shown in Figures 4.1 and 4.2 The figures show 2 of the 3 examples of Gaussian and error functions, wherein all the parameters are kept constant, except the standard deviation (σ). The first set (Fig 4.1) had the standard deviation as $\sigma = 25$; had $\sigma = 50$, and the third (Fig 4.2) as $\sigma = 100$. The mean is fixed at $\mu = -500$ units; the number of points in each of the functions is kept constant at 600, and the step of incrementing,

deltaH was fixed to 1 in all the examples. The fist component, i.e. the constant term of the FFT is omitted, as it carries no information. It is a sum of all the components. Also only the first 100 components are plotted, as these are coming from the FFT method, and correspond to imaginary negative harmonics. As the value of σ is increased, it was observed that the width of the Gaussian in the FFT also increased. The FFT of a Gaussian is also a Gaussian. It can be observed from the figures of the FFTs of the Gaussian that the FFT of the Gaussian with σ =25 is denser. Every second component of the FFT of the Gaussian with σ =25 is same as that in the FFT of the Gaussian with σ =50, and every fourth component is same as that in the FFT of σ =100. Homogeneous materials have a narrower distribution. i.e. the sigma is smaller in the gaussian, then it is wider in the *erf*, and vice versa.

4.2.2. Effect of varying the limits of the Gaussian and the error function

In order to optimize the measurement of hysteresis data, the effect of the number of data points and the maximum applied field after saturation, i.e. the measurement limits were investigated numerically. Figures 4.3, 4.4, and 4.5 show 3 examples of the Gaussian and error functions where all the parameters are kept constant, except the number of the "measured" points in the functions. The first set has a Gaussian and an error function, consisting of 300 points, the second has 600 points, and the third one has 1200 points. The standard deviation is kept constant at σ = 50, the mean is fixed at μ= –500 units, and the step of incrementing, *deltaH* is fixed to 1 in all the examples. Hence to change the number of points, the limits of the functions, i.e. the measurement field range, are varied. Another way of interpreting this would be that we are observing the change in FFT as we go deeper into the saturation region, i.e. $\pm 3\ \sigma$ in the first set, $\pm 6\ \sigma$ in the second set, and $\pm 12\sigma$ in the 3rd set. The fist component of the FFT is omitted, as it carries no information. It is a sum of all the components. Also only the first 100 components are plotted as the second half is a mirror image of these and the ones omitted are insignificant to make a difference. It can be observed that for the Gaussian, the first component (first component in the graph plotted) in the set for 300 points (Fig 4.3) is the same as the second component in the respective FFTs of the 600-point set (Fig 4.4) and 3rd component of that in the 1200 point set (Fig 4.5). Thus in case of the Gaussian, the more we go into the saturation region, the more intermediate components we get. However in case of the error function, the FFT for 300 points, i.e, $\pm\ 3\ \sigma$ seems to have a smoother shape than the rest. As we go more into saturation, the low order components seem to fluctuate in magnitude. Also the first component in the FFT of the error function increases significantly in magnitude as we go deeper into saturation. The second component however remains constant at a magnitude of 20.

4.2.3. Effect of varying the number of samples in the Gaussian and error function

To optimize the time, needed for hysteresis measurements, the number of data points taken should be determined. To model this effect, *deltaH*, the incremental magnetic field step was changed, thus varying the number of samples in the Gaussian and error function. The effect on the FFT was analyzed. Figures 4.5, 4.6, and 4.7 show 3 examples of Gaussian and error functions wherein all the parameters are kept constant, except *deltaH*. Hence this in effect is related to changing the number of points in the functions. The value of *deltaH* is kept 1 in the first case (Fig 4.5), 2 in the second (Fig 4.6) and 4 in the third (Fig 4.7). As the limits of the function are kept fixed from H=–1200 to 200, varying *deltaH* is effectively varying the number of points in the functions from 1200 in the first one to 600 in the second, and 300 in the third .It can seen from the figures that the FFTs are similar for the three sets. However the magnitude of each component doubles as *deltaH* halves.

4.2.4. Effect of varying the mean value

The mean value of the Gaussian and the *erf* corresponds to the coercivity on the magnetic hysteresis. Coercivity is very sensitive to microstructure and the technology of preparation of a magnetic material; therefore it is very important to see the effect of its change on the FFT. Figure 4.8. shows the phase of the first 6 harmonics of the FFT of the measured DELTACARDS and METROCARDS (See details in Section 6). Interesting to note that the odd harmonics differ for the very similar samples of these sets, while the even harmonics are very close for all. The numerical values of the phases are distinct. Figures 4.9 and 4.10 show 2 examples of Gaussian and error function wherein all the parameters are kept constant, except the mean value of

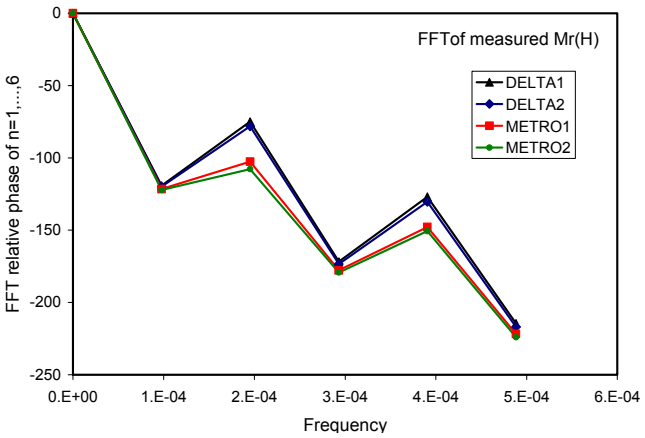

Fig. 4.8. The frequency dependence of the phase of the measured 2 groups of magnetic materials. The first 6 harmonics are shown, const term included. (ORIGINPro7)

the functions (H_c). The mean is varied from –500 in the first set (Fig. 4.9.), to –2500 in the next set (Fig. 4.10.), corresponding to semihard magnetic materials as in credit cards and magnetic recording media). The results of the FFT of the Gaussians and error functions are identical. Hence it can be stated that the mean of the functions doesn't have any effect on the FFT magnitudes, but it shows up in the phase. However the relative mean values between 2 overlapped Gaussians affects the resultant FFT. This is explained in the next section.

4.2.5. Effect of varying the magnitude of the functions

The magnitude of the *erf* function corresponds to the remanent magnetization of the material under test.. Usually, larger M_r means larger saturation magnetization, M_s. The effect of the change of the magnetization can be modified by increasing the magnitude of the functions by a particular factor. It can be seen that the same factor for both the error function and Gaussian magnifies the respective components in the FFT.

4.3. Conclusions

It was shown that the Discrete Fourier Transformation (DFT) of the DC remanent hysteresis loops is very sensitive to the parameters of the magnetic measurements. Special care has to be taken when measuring materials to be analyzed, compared, and identified. In this work the FFT algorithm of the MATLAB package was used to obtain the DFT coefficients, although many other FFT algorithms are available, as part of a bigger software package. The measurement protocol should require that all/both samples were measured the same way:

1. The limits of the measurements, i.e. the largest applied field, H_{max}, should kept constant, i.e. the period *T=constant*;
2. The field step, *deltaH*, i.e. the number of data points, should be kept constant for all samples and during the whole hysteresis measurement; i.e. the sampling rate N/T = const for all samples;
3. The same FFT algorithm should be used for the evaluation of the data.

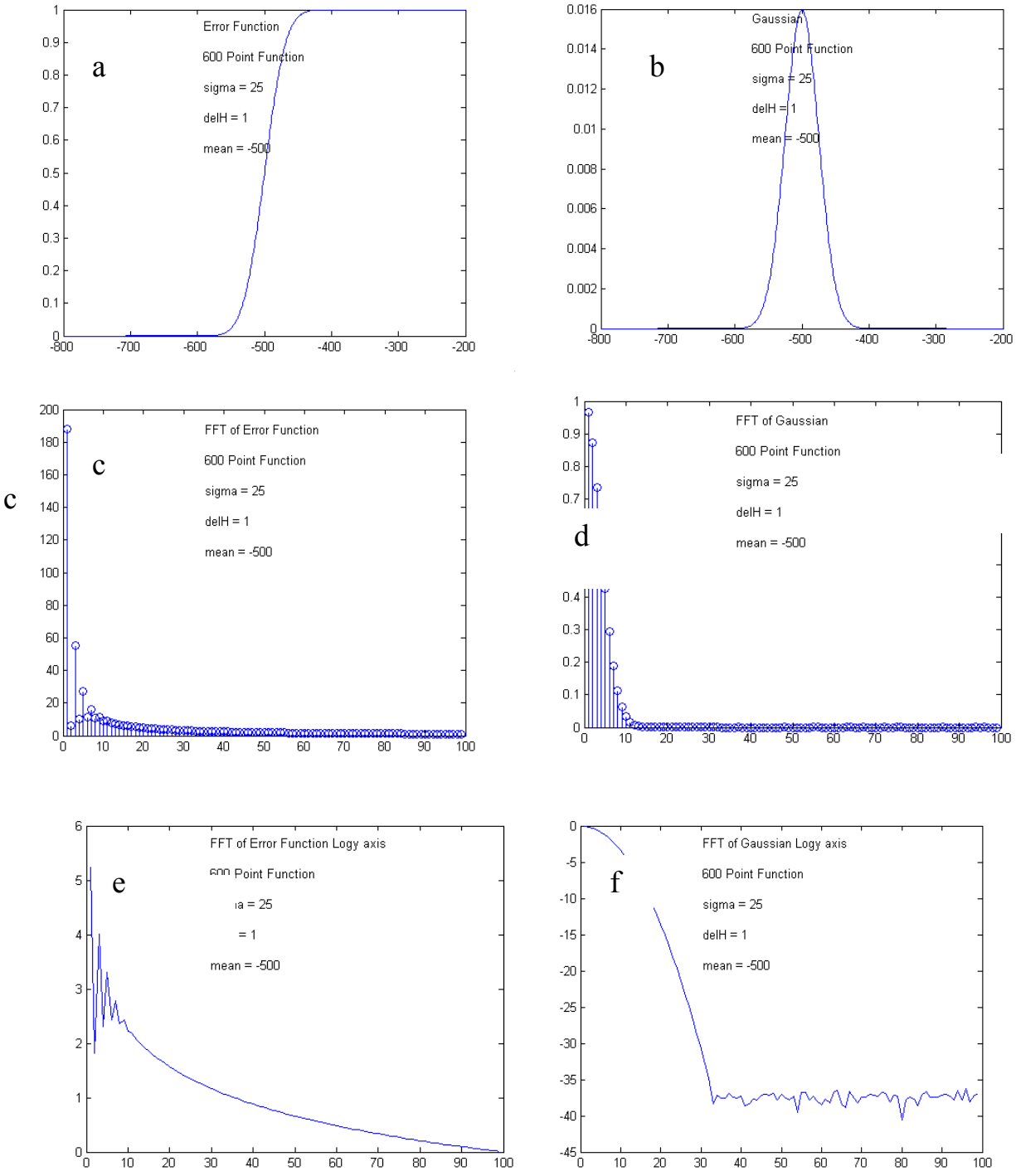

Fig 4.1 Effect of model parameters on FFT. Effect of varying the standard deviation σ on FFT: (a) – *erf* ; (b) – Gaussian function; (c) – FFT of *erf*; (d) – FFT of Gaussian Function; (e) – FFT of *erf,* magnitude in *Log* axis; (f) – FFT of Gaussian, magnitude in *Log* axis. σ =25, H_c = -500 Oe, # of points in both Gaussian and *erf*= 600.

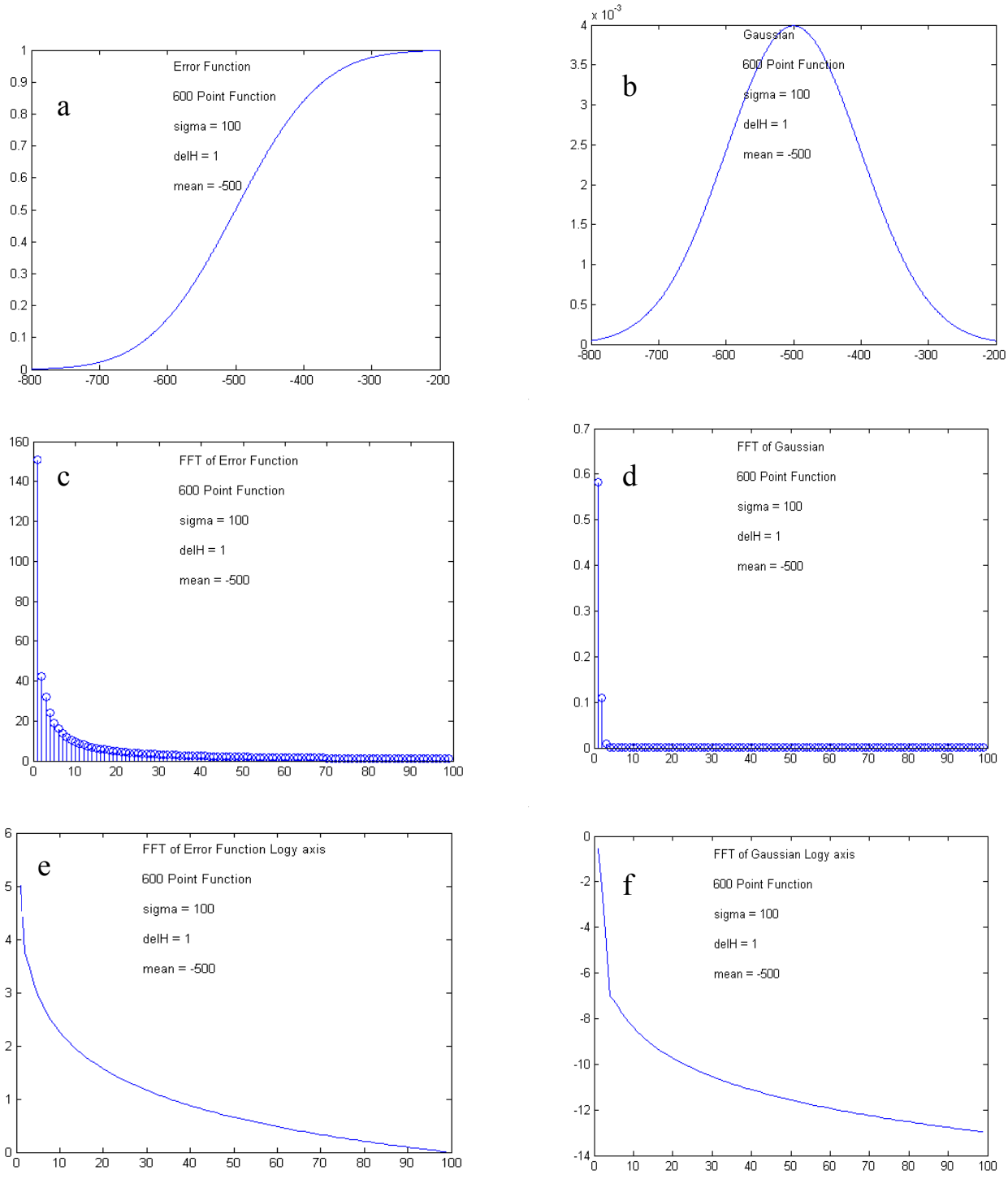

Fig 4.2 Effect of model parameters on FFT. Effect of varying the standard deviation σ on FFT. (a) – *erf* ; (b) – Gaussian function; (c) – FFT of *erf*; (d) – FFT of Gaussian Function; (e) – FFT of *erf,* magnitude in Log axis; (f) – FFT of Gaussian, magnitude in Log axis. σ =100, H_c = -500 Oe, # of points in both Gaussian and *erf*= 600.

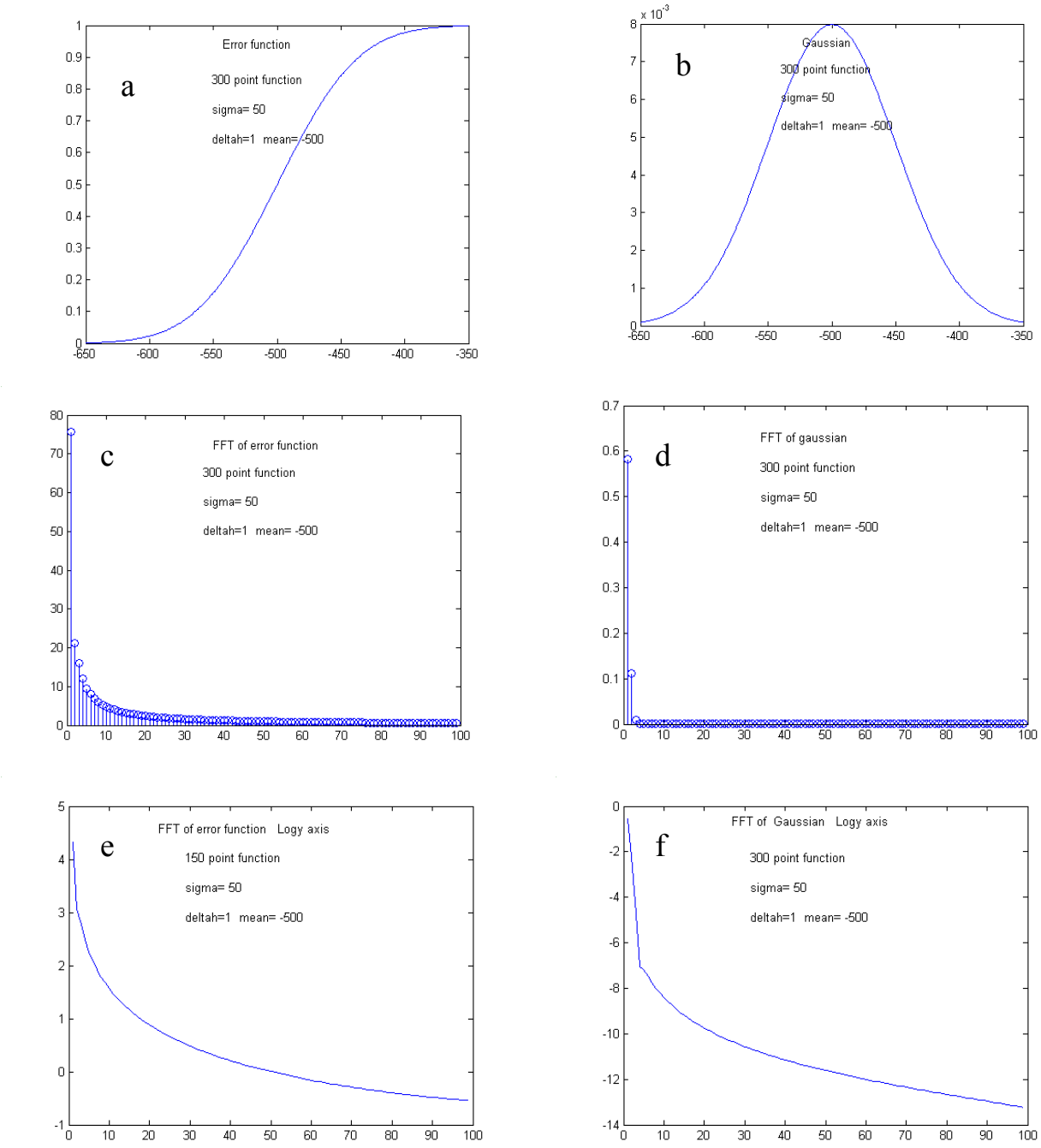

Fig. 4.3. Effect of model parameters on FFT. Effect of varying the limits of Gaussian and error function: (a) – *erf* ; (b) – Gaussian function; (c) – FFT of *erf*; (d) – FFT of Gaussian; (e) – FFT of *erf,* magnitude in Log axis; (f) – FFT of Gaussian, magnitude in Log axis. σ =50, H_c = -500 Oe, # of points in both Gaussian and *erf*= 300.

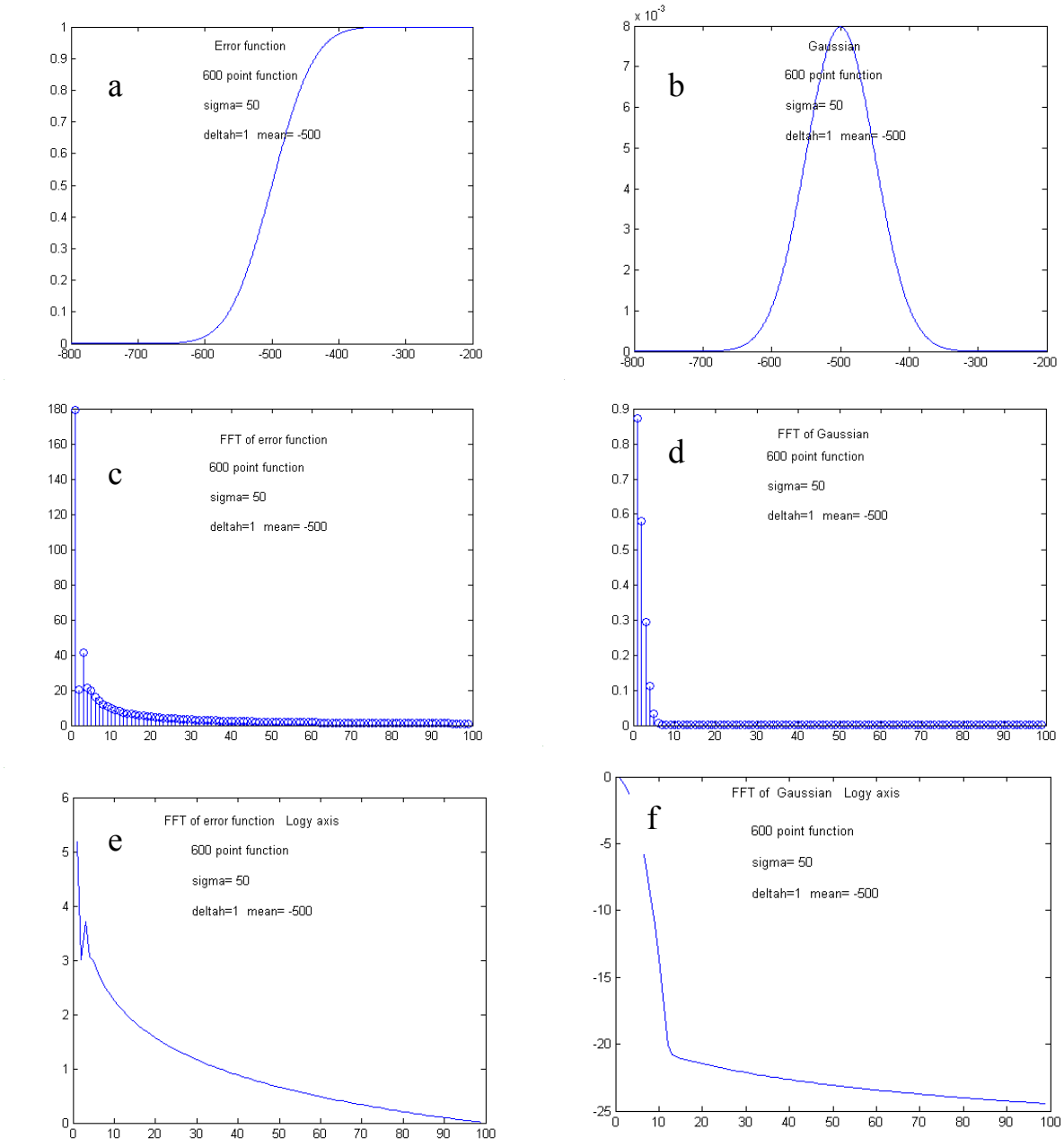

Fig 4.4. Effect of model parameters on FFT. Effect of varying limits of Gaussian and error function: (a) – *erf* ; (b) – Gaussian function; (c) – FFT of *erf*; (d) – FFT of Gaussian; (e) – FFT of *erf,* magnitude in Log axis; (f) – FFT of Gaussian, magnitude in Log axis. σ =50, H_c = -500 Oe, # of points in both Gaussian and *erf*= 600.

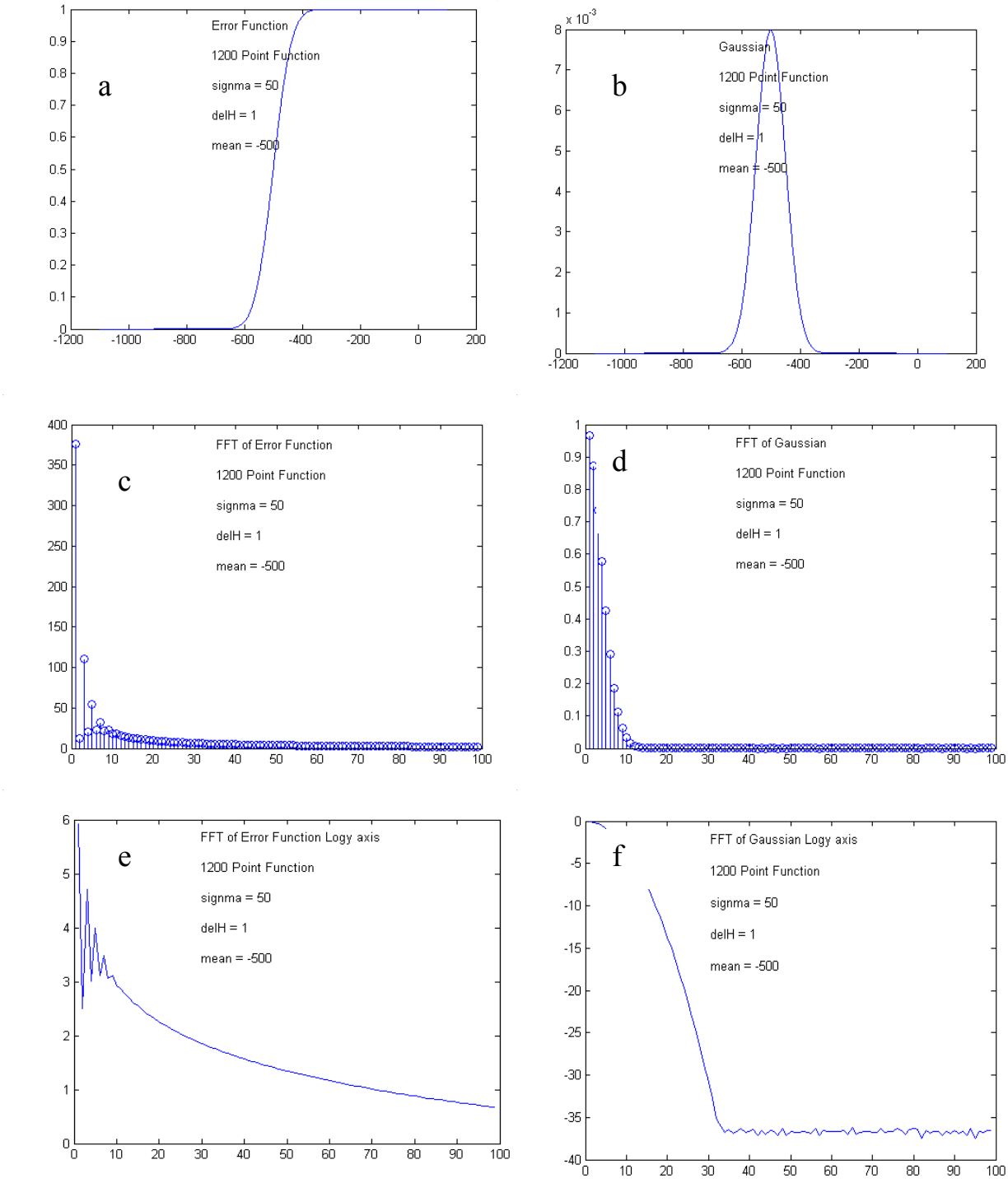

Fig 4.5 Effect of model parameters on FFT. Effect of varying *deltaH* (step of increment). (a) – *erf* ; (b) –Gaussian Function; (c) – FFT of *erf*; (d) – FFT of Gaussian; (e) – FFT of *erf,* magnitude in Log axis; (f)– FFT of Gaussian, magnitude in Log axis. σ =50, H_c = -500 Oe, # of points in both Gaussian and *erf*= 1200, *deltaH* =1.

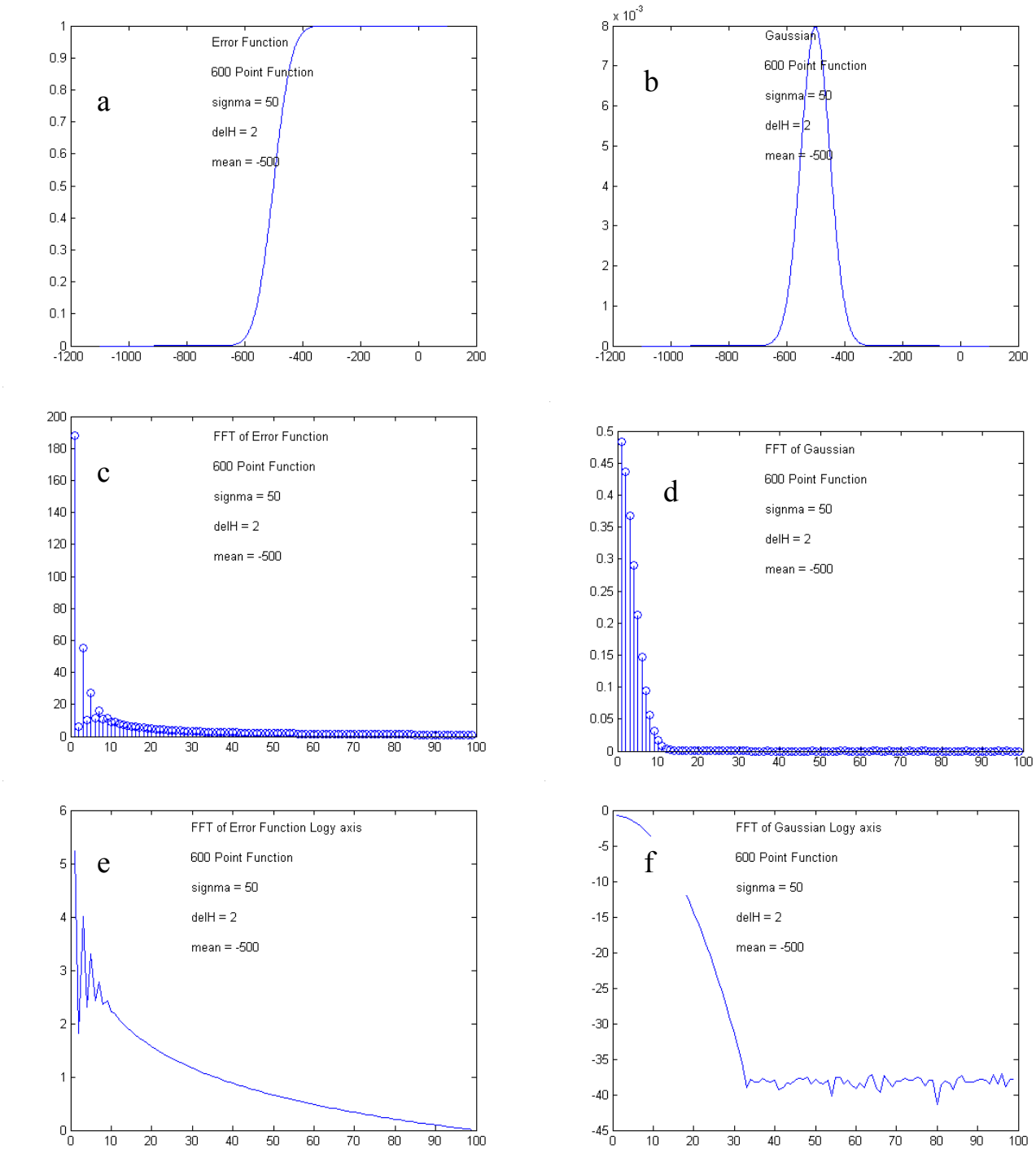

Fig. 4.6. Effect of model parameters on FFT. Effect of varying *deltaH* (step of increment). (a) – *erf*; (b) –Gaussian Function; (c) – FFT of *erf*; (d) – FFT of Gaussian ; (e) – FFT of *erf,* magnitude in Log axis; (f) – FFT of Gaussian, magnitude in Log axis. σ =50, H_c = -500 Oe, # of points in both Gaussian and *erf*= 600, *deltaH* =2.

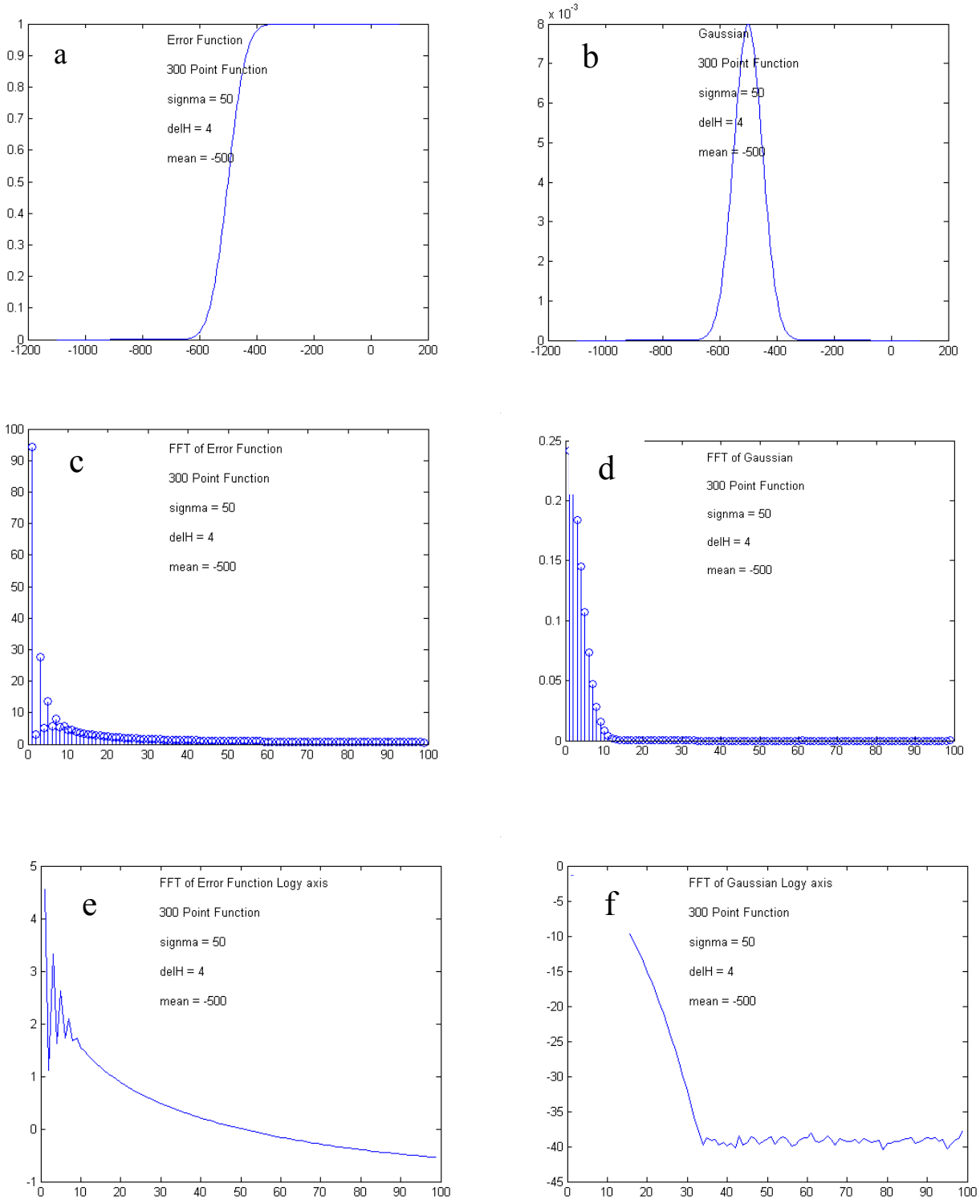

Fig 4.7. Effect of model parameters on FFT. Effect of varying *deltaH* (step of increment). (a) – *erf,* (b) Gaussian function; (c) – FFT of *erf*; (d) – FFT of Gaussian; (e) – FFT of *erf,* magnitude in Log axis; (f)– FFT of Gaussian, magnitude in Log axis. σ =50, H_c = -500 Oe, # of points in both Gaussian and *erf*= 300, *deltaH*= 4.

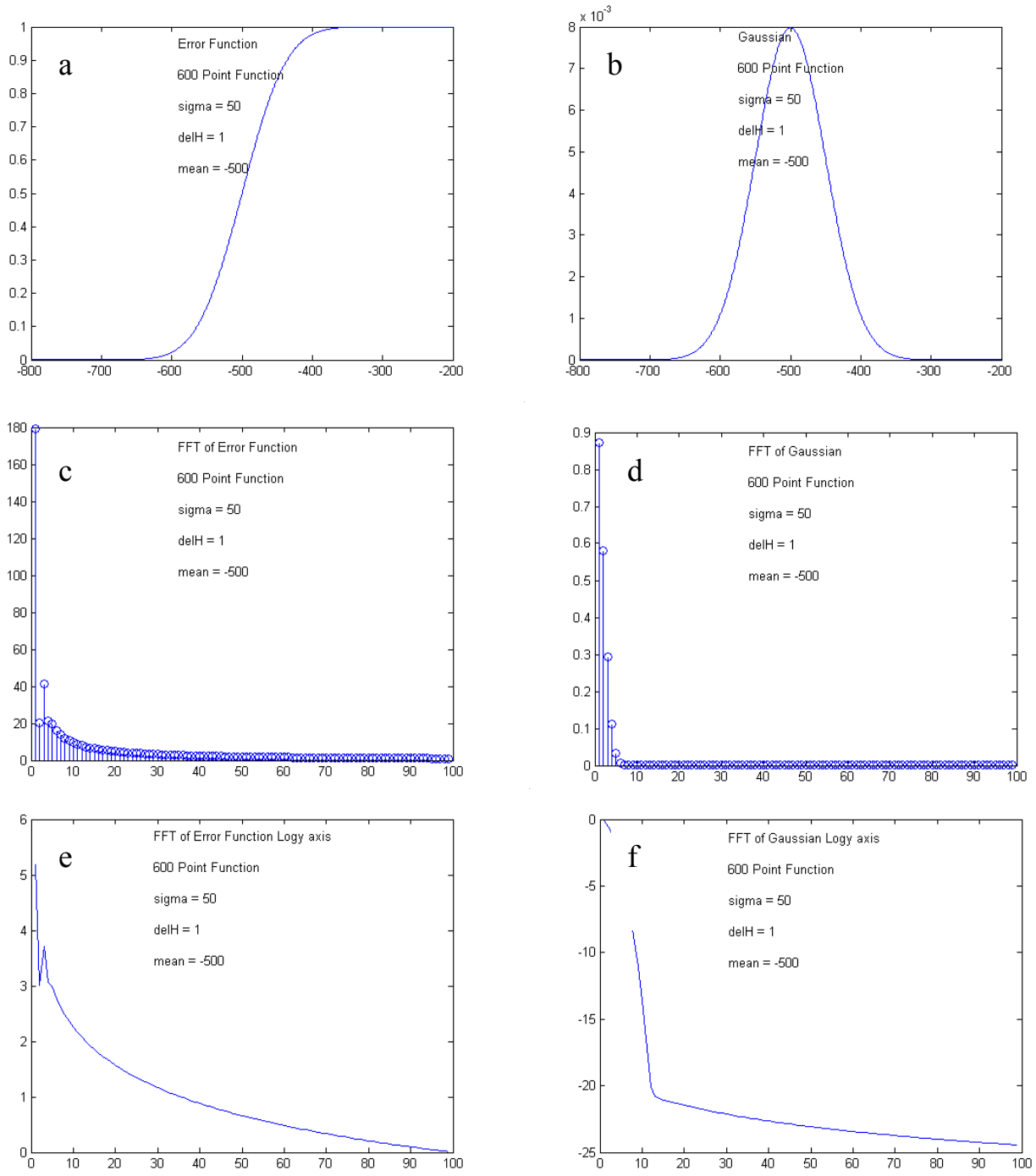

Fig. 4.9. Effect of model parameters on FFT; Effect of varying the mean value (H_c)of the Gaussian and *erf*. (a) – *erf* ; (b) – Gaussian function; (c) – FFT of *erf*; (d) – FFT of Gaussian; (e) – FFT of *erf,* magnitude in Log axis; (f)– FFT of Gaussian, magnitude in Log axis. σ =50, # of points in both Gaussian and *erf*= 600, H_c = -500 Oe.

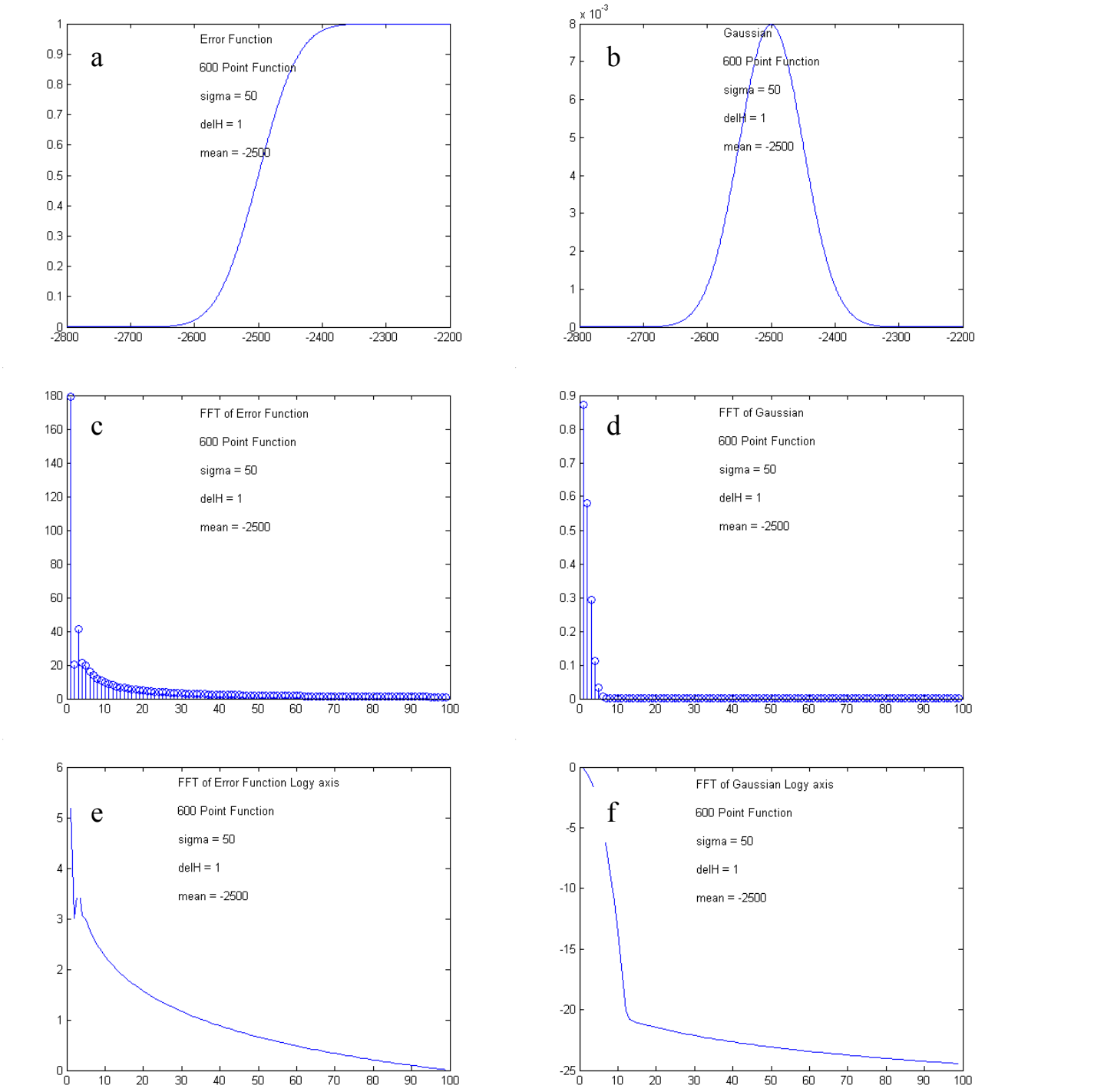

Fig. 4.10 Effect of model parameters on FFT. Effect of varying the mean value (H_c) of the Gaussian and *erf*: (a) – *erf* (b) – Gaussian; (c) –FFT of erf ; (d) – FFT of Gaussian; (e) –FFT of *erf,* magnitude in Log axis; (f) –FFT of Gaussian, magnitude in Log axis; σ =50, # of points in both Gaussian and *erf*= 600 H_c = -2500 Oe.

5. SENSITIVITY OF FFT TO MAGNETIC MARKERS

Magnetic markers are used for fraud and theft prevention, identification, in security tags, in bank checks, and as currency markers. A numerical simulation of the effect of a magnetic marker, inserted into a magnetic material, on the FFT of the RHL was carried out. The simulation involves the hysteresis loop and the SFD of two different magnetic materials. The matrix has certain coercivity, amount and/or magnetization, and a certain distribution of the properties, modeled with σ being the standard deviation, μ the mean value of then distribution, which is the coercivity, H_c, and x, corresponding to the applied magnetic field H. A marker is a highly homogeneous material with a very narrow switching field distribution.

The relative position of the mean value of the marker with respect to the matrix, and the difference in distribution width was varied. The sum of two Gaussians is also a Gaussian, and from the linearity of FFT it follows that the FFT follows this rule. If two magnetic materials with similar properties and similar in amounts, are mixed together, the measured hysteresis loop and its FFT won't reveal that the material is a mixture. However, when placing a small amount of material with very different properties into the matrix, the presence of the marker won't be seen in the usual magnetic hysteresis measurement, but it could be identified from the FFT.

Simulations were performed to find the optimal position (coercivity) of the marker with respect to the mean H_c, and to define the smallest amount of the marker in % of the total magnetization. Hence a Gaussian and error function with $\sigma = 5$ are selected to represent a marker. Table I shows a few of the different combinations of parameters that were changed in the simulations. The results of the simulations of parameters in row 1 is illustrated in Fig 5.3. Figure 5.1 shows the FFTs of the Gaussian and error function selected to represent a standard magnetic material (matrix). The functions have 600 points, $\sigma = 50$, $\mu = -500$, and the amount of magnetization (Amplitude) A = 1. Fig 5.2 shows the FFT of the marker material. This has 600 points, $\sigma = 5$, $\mu = -500$, and A = 1. Fig 5.3 shows the FFT of the mixture of the two materials, containing equal amounts of marker material and sample magnetic material. (Fig 5.3 thus represents the sum of a matrix shown in Fig 5.1 and a marker of Fig 5.2, taken in equal amounts.) Due to the linearity of FFT, The FFTs of the Gaussian and error function are a sum of the respective FFTs of the sample and the marker. For example the first component in Fig 5.1c is 180 units in magnitude and in Fig 5.2c it is 190 units. Hence the first component in Fig. 5.3c is 370 units in magnitude. The same is true for all the other components.

5.1. Effect of varying the ratio of matrix to marker

The simulations of rows 2, 3 and 4 of Table I are shown in Figures 5.4, 5.5, and 5.6. These show the FFTs of the different proportions of the marker with respect to the matrix material. Fig 5.4 shows the matrix when both the constituent materials are equal in proportion (i.e.A1=A2=1) hence the amount of phase 1=50% and that of phase2=50%.

Fig 5.5 shows the matrix when amount of phase 1=83% and the amount of phase2=17%. (i.e. A1 =1, A2=0.2). Fig 5.5 illustrates the case when the amount of phase1 = 91%, and of phase2 = 9%. (i.e. A1 =1, A2=0.1). Fig 5.6 shows the composite when the amount of phase1 = 98% and of phase2 = 2%. (i.e. A1 =1,A2=0.01).

It can be seen that the FFT of Gaussian is more sensitive to the presence of marker than the FFT of the error function. This is probably due to the significant difference in the sigma (σ) of the two materials.

When Fig. 5.1 is compared with Figs 5.4, 5.5 and 5.6, it can be seen that as the concentration of the marker material falls below 10%, the FFT of the error function is almost similar to that of the original sample (Fig.5.1c). The difference is then seen only in the FFT of the Gaussian.

The FFT spectrum in a logarithmic scale gives a better picture of the minute differences. The numerical values of the FFT coefficients (amplitude and phase) carry more information than the Figures, however, for illustrative purposes only the figures are shown.

5.2. Effect of varying the coercivity (mean value of distribution) of the marker

Rows 5, 6, and 7 in Table I represent 3 mixtures, all having the same amount of sample material (83%) and that of the marker (17%) in the matrix (A1=1 A2=0.). Two of these simulations are illustrated in fig 5.7 and 5.8. The mean value of the marker's distribution is varied in the three sets. i.e H_{c2} = -505 in row5 (Fig 5.7), H_{c2} = -525 in row 6 , and H_{c2} = -600 in row 7 (Fig 5.8). It can be seen that there is only a slight difference in the FFTs of the error function on varying the mean of the marker material. Results of simulations of rows 5 and 6 are almost identical. This is also due to the fact that the mixture contains only 17% of marker material. Hence the difference in the FFT shows up only when there is a large difference in the means of the constituent materials as in row 7 (Fig 5.8), where the difference in the means is 100 units. Hence the difference is seen in the FFTs. The difference is more prominent in the FFT of the Gaussian. In general, only the first few components of the FFT of the Gaussian, corresponding to the SFD of the RHL, show the difference. The higher order components of both the error function and Gaussian do not show any difference, as they are too small to affect the sum due to the shift.

It can be concluded that to observe a significant change in the FFT of error function, either the amount of the marker material should be high enough (about20%) in case when the marker is close to the matrix, or the mean (the coercivity (H_c) of the marker material should be far apart from that of the sample material if the concentration of the marker material in the matrix is less than 10%). That is the best results are abstained for a small amount of a marker (≤10%), having a narrow SFD, and coercivity inside the tail of the Gaussian SFD of the matrix.

It is proposed to perform experimental investigation on matrix-marker magnetic nanocomposite systems to establish the minimum amount and optimal properties for a marker material relative to the matrix.

Table I
Sensitivity of FFT to magnetic markers

Coercivity of matrix, mean (H_{c1})	Coercivity of marker mean (H_{c2})	Standard deviation of matrix ($\sigma 1$)	Standard deviation of marker ($\sigma 2$)	Amount of matrix (A1)	Amount of marker (A2)
-500	-500	50	5	1	1
-500	-525	50	5	1	0.2
-500	-525	50	5	1	0.1
-500	-525	50	5	1	0.05
-500	-505	50	5	1	0.2
-500	-525	50	5	1	0.2
-500	-600	50	5	1	0.2

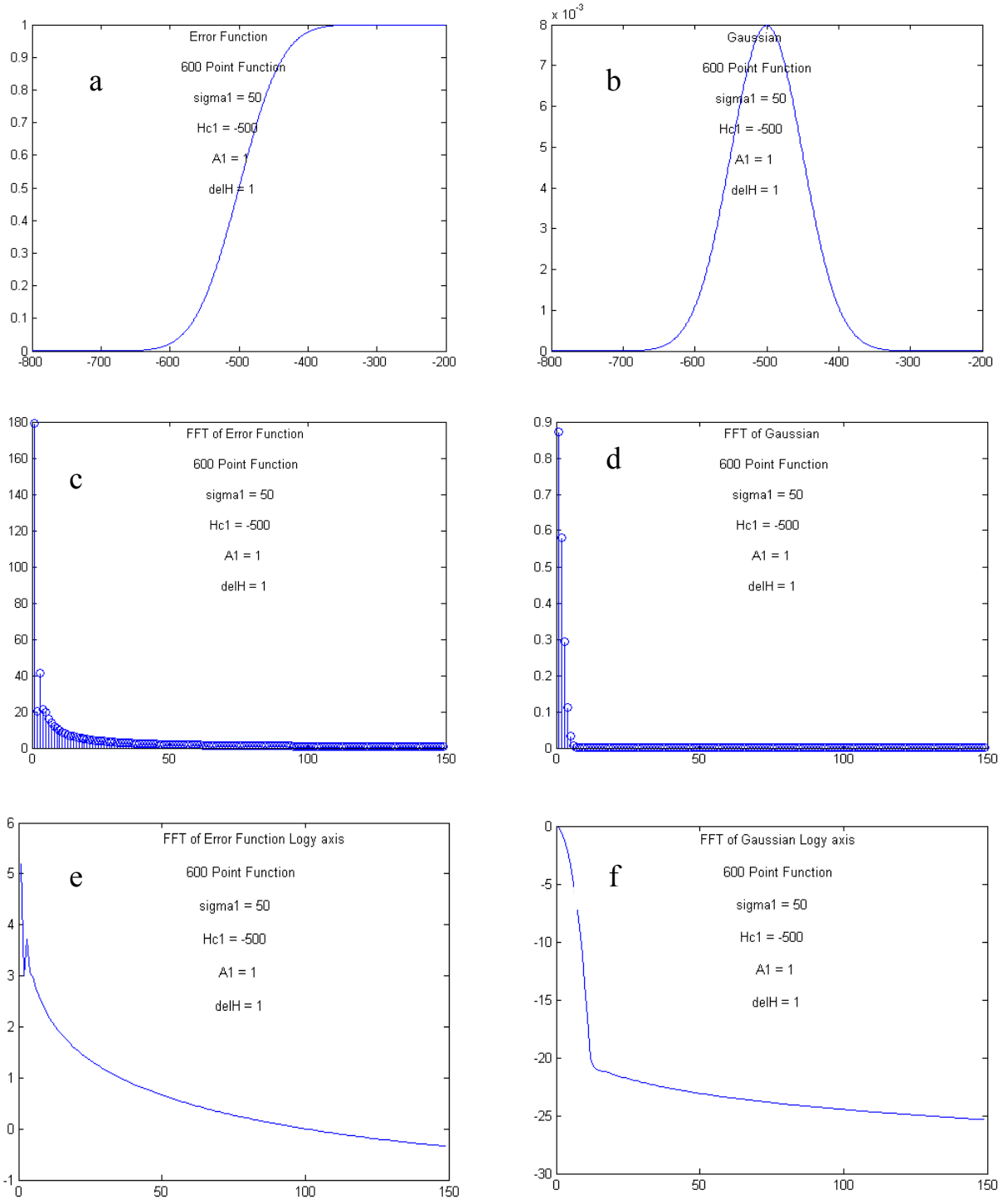

Fig 5.1 Sensitivity of FFT to magnetic markers. FFT of the matrix magnetic material. (a) – the *erf* of the matrix, (b) – Gaussian function; (c) – FFT of *erf*; (d) – FFT of Gaussian function; (e) – FFT of erf, magnitude in log axis; (f) – FFT of Gaussian in log axis . σ =50 , H_c = -500 Oe.

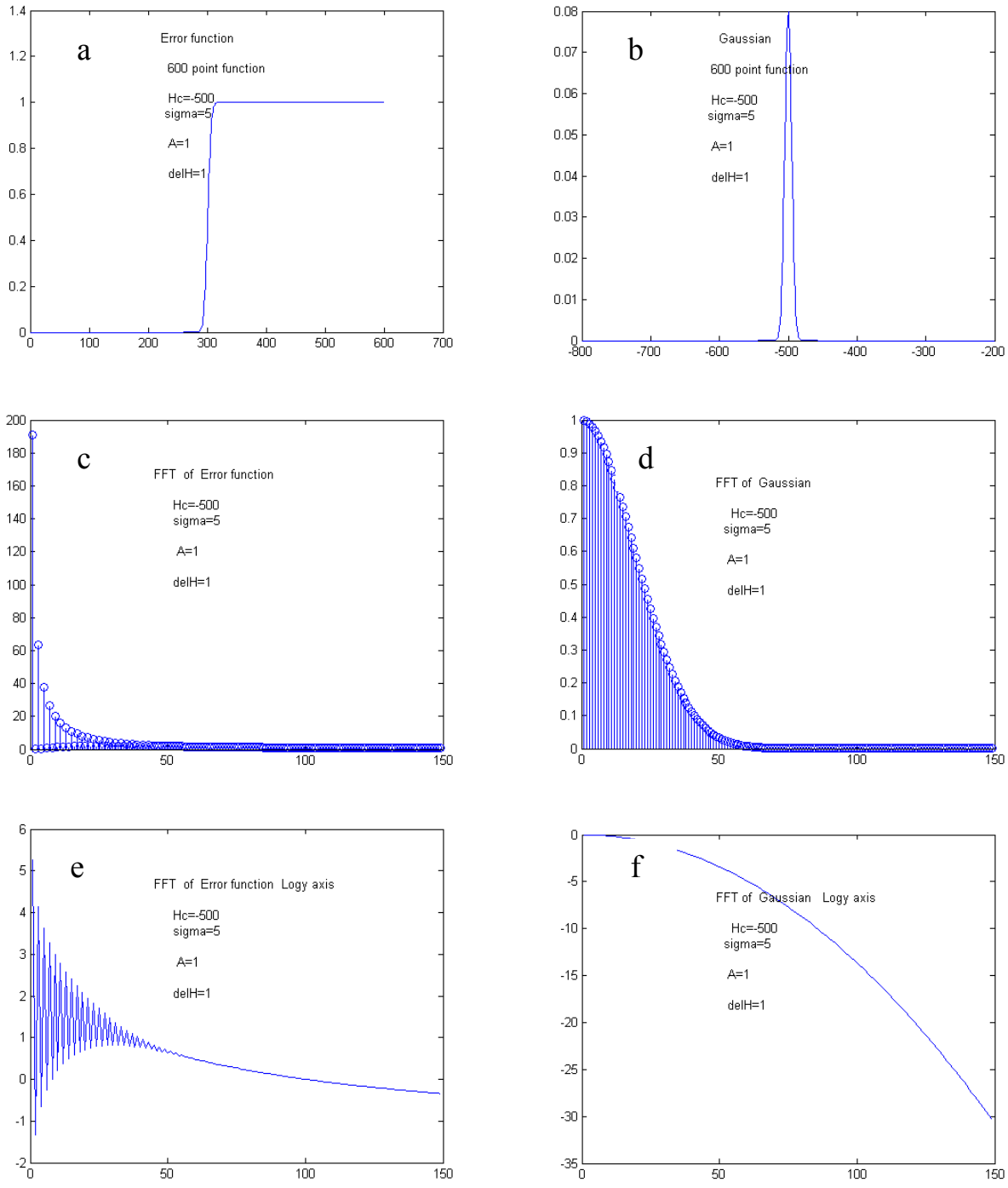

Fig 5.2 Sensitivity of FFT to magnetic markers. FFT of the marker material. (a) – the *erf* of the marker; (b) – Gaussian function; (c) – FFT of *erf*; (d) – FFT of Gaussian function; (e) – FFT of *erf,* magnitude in log axis; (f) – FFT of Gaussian in log axis $\sigma = 5$, $H_c = -500$ Oe.

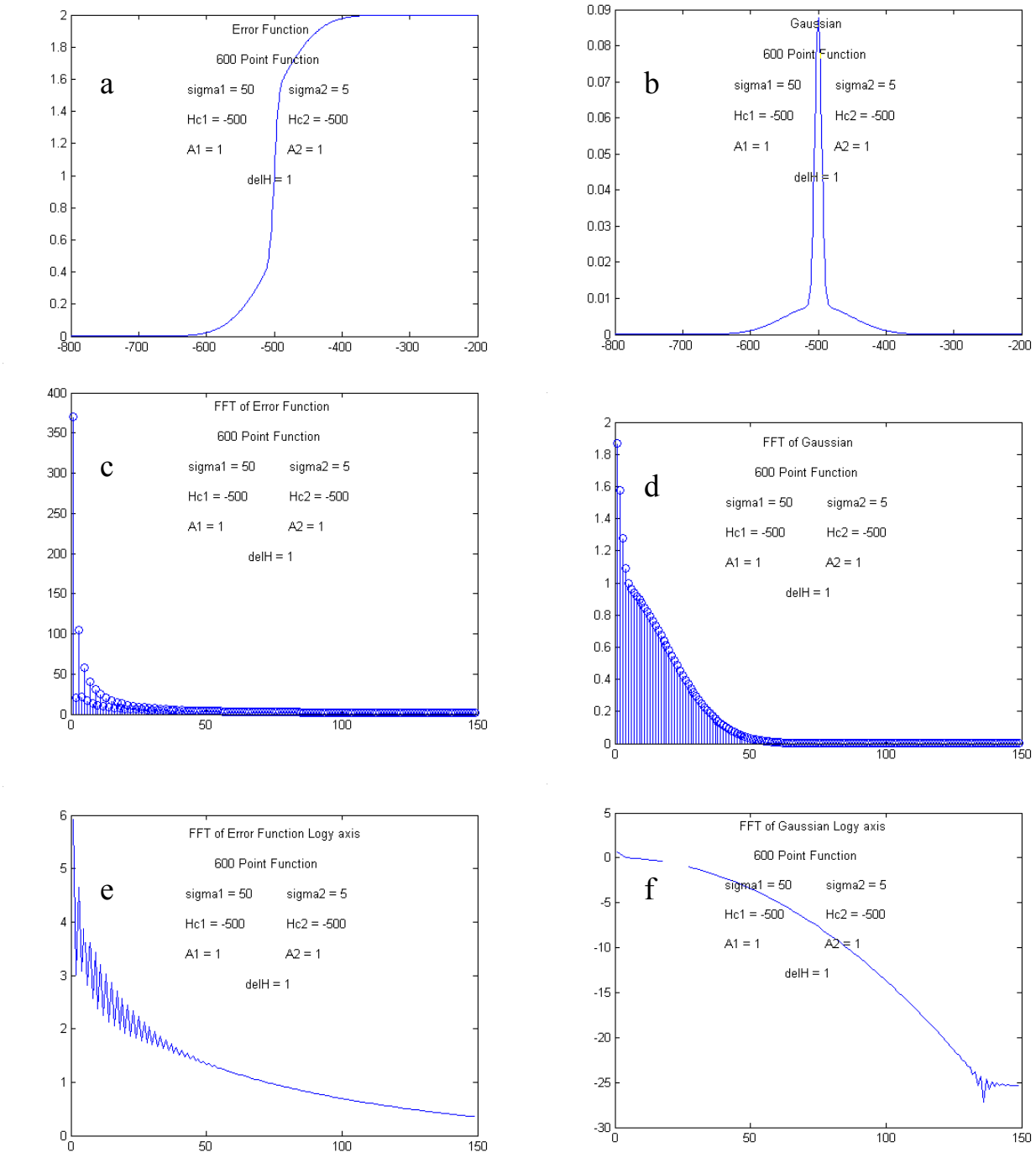

Fig 5.3 Sensitivity of FFT to magnetic markers. FFT of the composite material; Amount Phase 1 = 50% Phase 2 = 50%. (a) – the *erf* of the matrix; (b) – Gaussian function; (c) – FFT of *erf*; (d) – FFT of Gaussian function; (e) – FFT of erf, magnitude in log axis; (f) – FFT of Gaussian in log axis . ; σ_1 =50 Hc_1 = -500 Oe A1=1, σ_2 =5 H_{c2} = -500 Oe A2=1

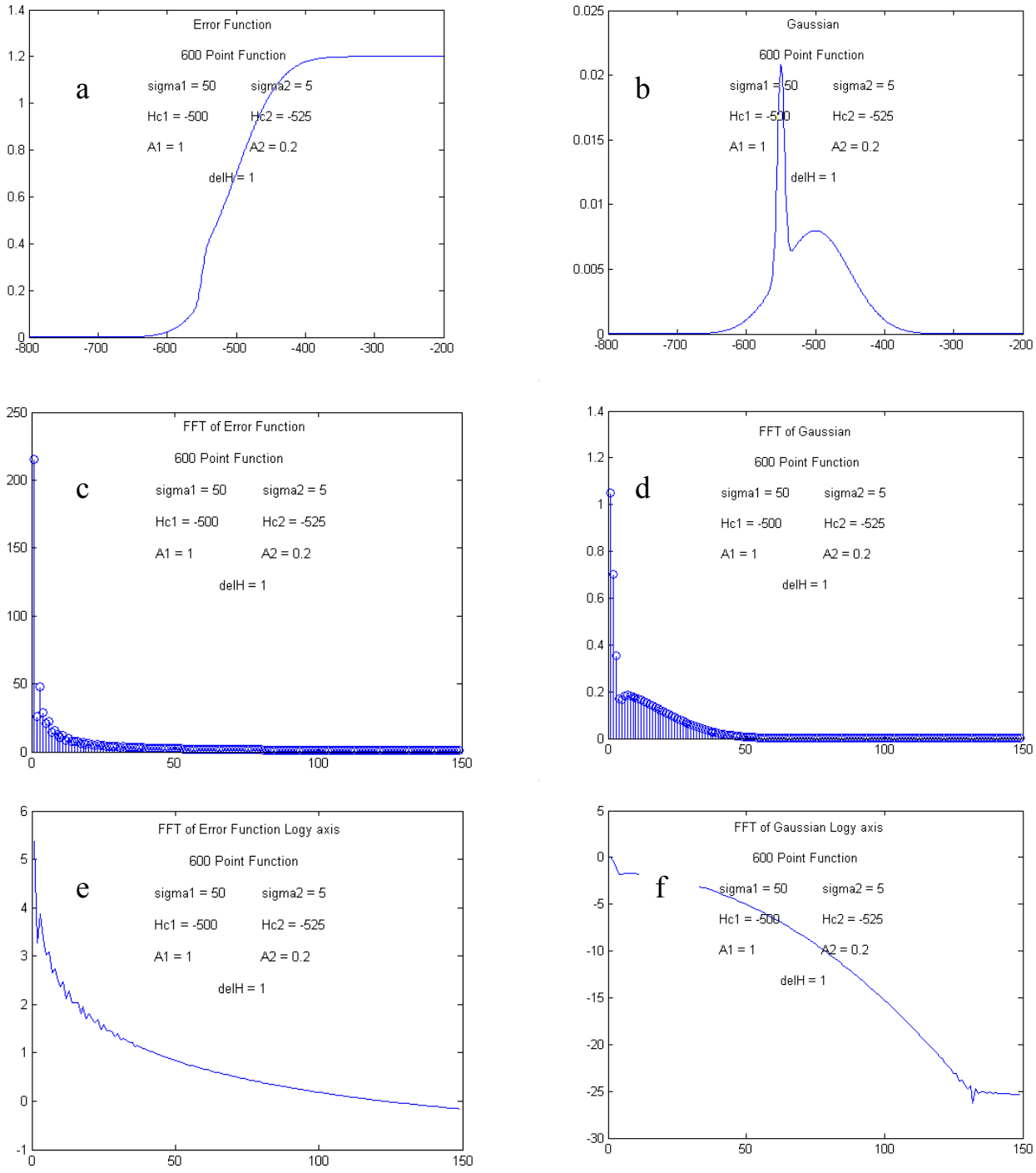

Fig 5.4. Sensitivity of FFT to magnetic markers. FFT of the composite material ; Effect of varying the ratio of sample to marker on the FFT; amount Phase 1 = 83% Phase 2 = 17%. (a) – the *erf* of the matrix; (b) – Gaussian function; (c) – FFT of *erf*; (d) – FFT of Gaussian function; (e) – FFT of erf, magnitude in log axis; (f) – FFT of Gaussian in log axis . ; σ_1 =50 H_{c1} = -500 Oe A1=1, σ_2 =5 H_{c2} = -525 Oe A2=0.2

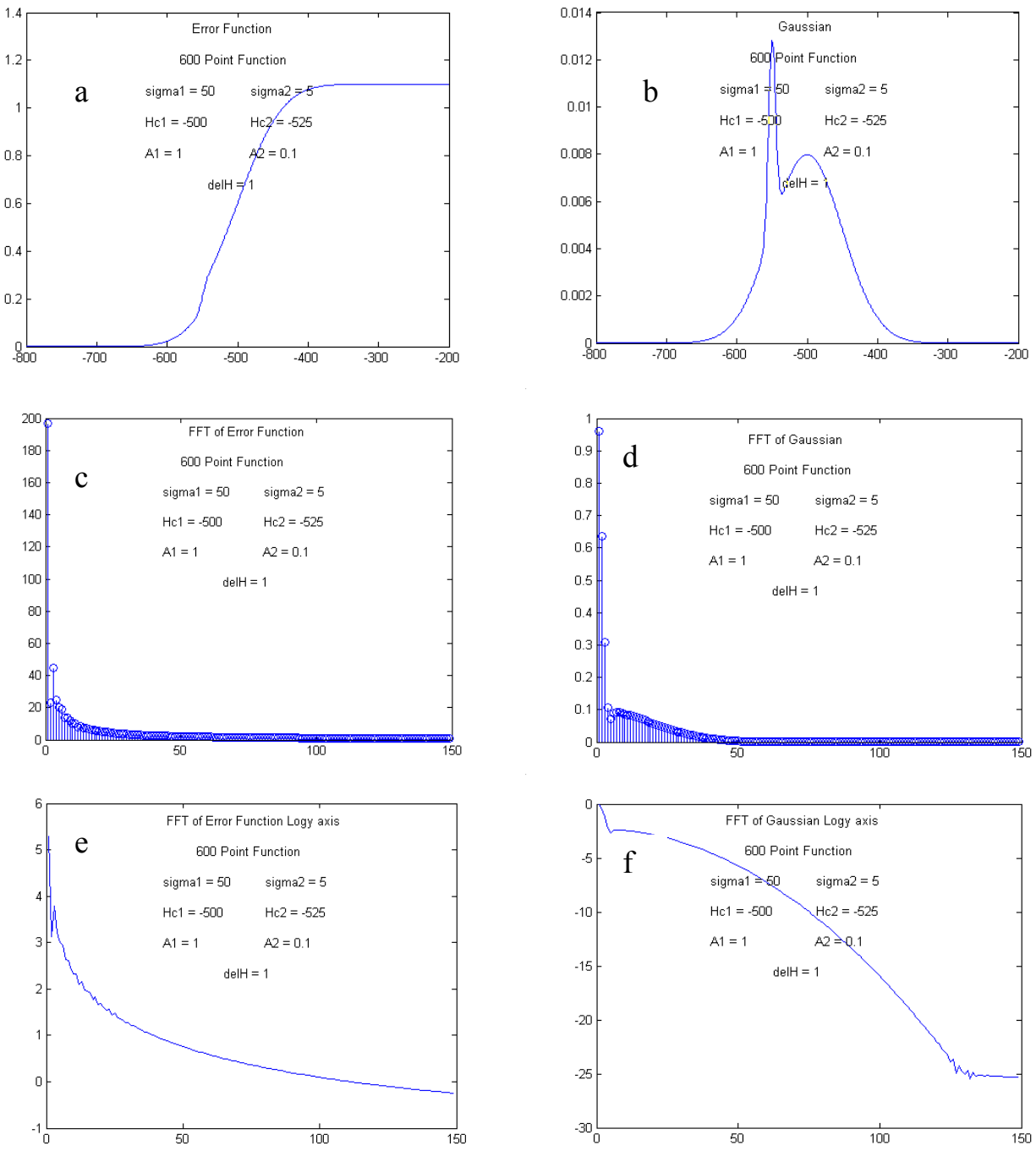

Fig 5.5. Sensitivity of FFT to magnetic markers. FFT of the composite material; Effect of varying the ratio of sample to marker on the FFT; amount Phase 1 = 91%, Phase 2 = 9%. (a) – the *erf* of the matrix; (b) – Gaussian function; (c) – FFT of *erf*; (d) – FFT of Gaussian function; (e) – FFT of erf, magnitude in log axis; (f) – FFT of Gaussian in log axis . ; σ_1 =50 H_{c1} = -500 Oe A1=1, σ_2 =5 H_{c2} = -525 Oe A2=0.1

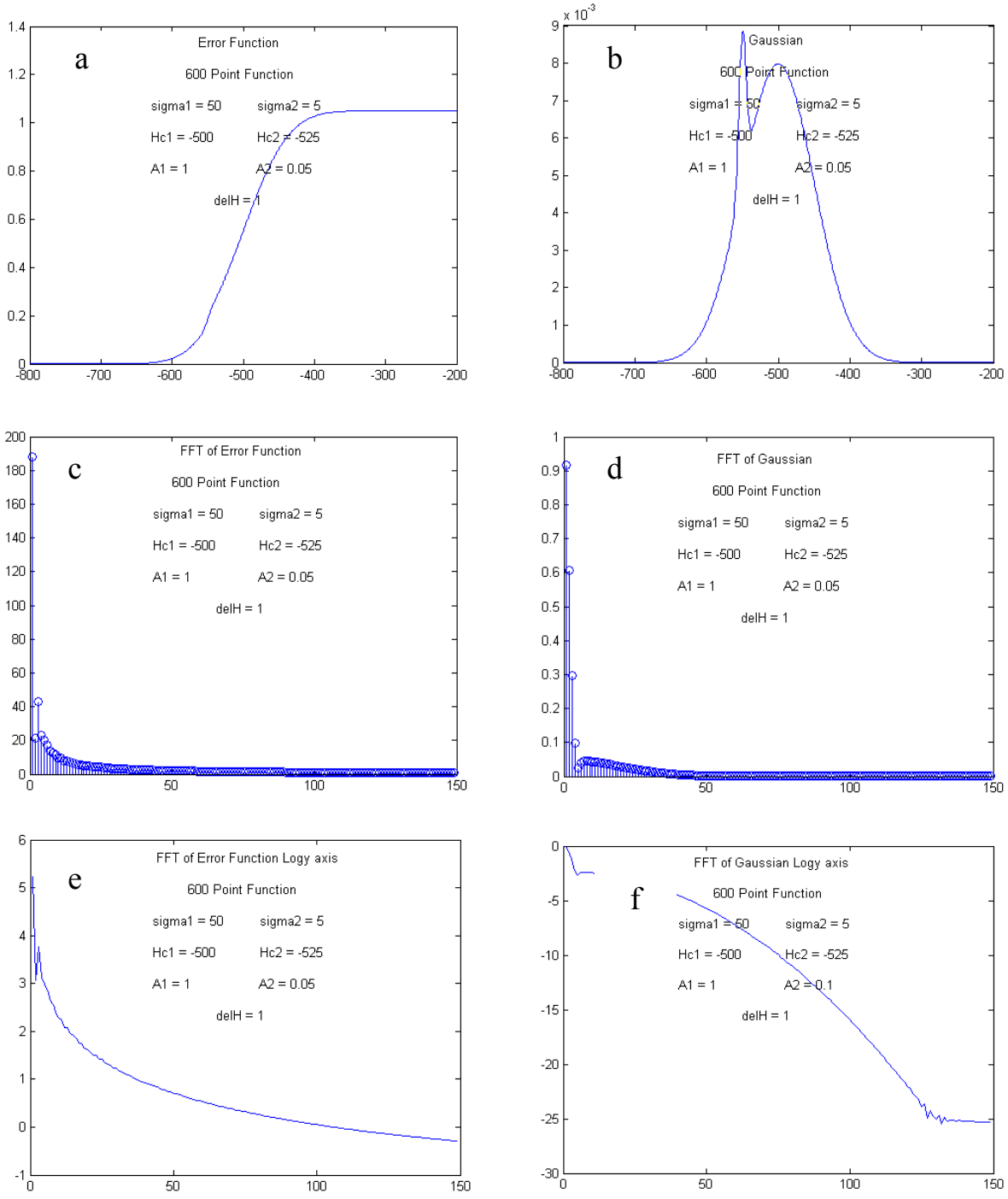

Fig 5.6. Sensitivity of FFT to magnetic markers. FFT of the composite material; Effect of varying the ratio of sample to marker on the FFT, Amount Phase 1 = 98%, Phase 2 = 2%. (a) – the *erf* of the matrix; (b) – Gaussian function; (c) – FFT of *erf*; (d) – FFT of Gaussian function; (e) – FFT of erf, magnitude in log axis; (f) – FFT of Gaussian in log axis . σ_1 =50 H_{c1} = -500 Oe A1=1, σ_2 =5 H_{c2} = -525 Oe A2=0.05

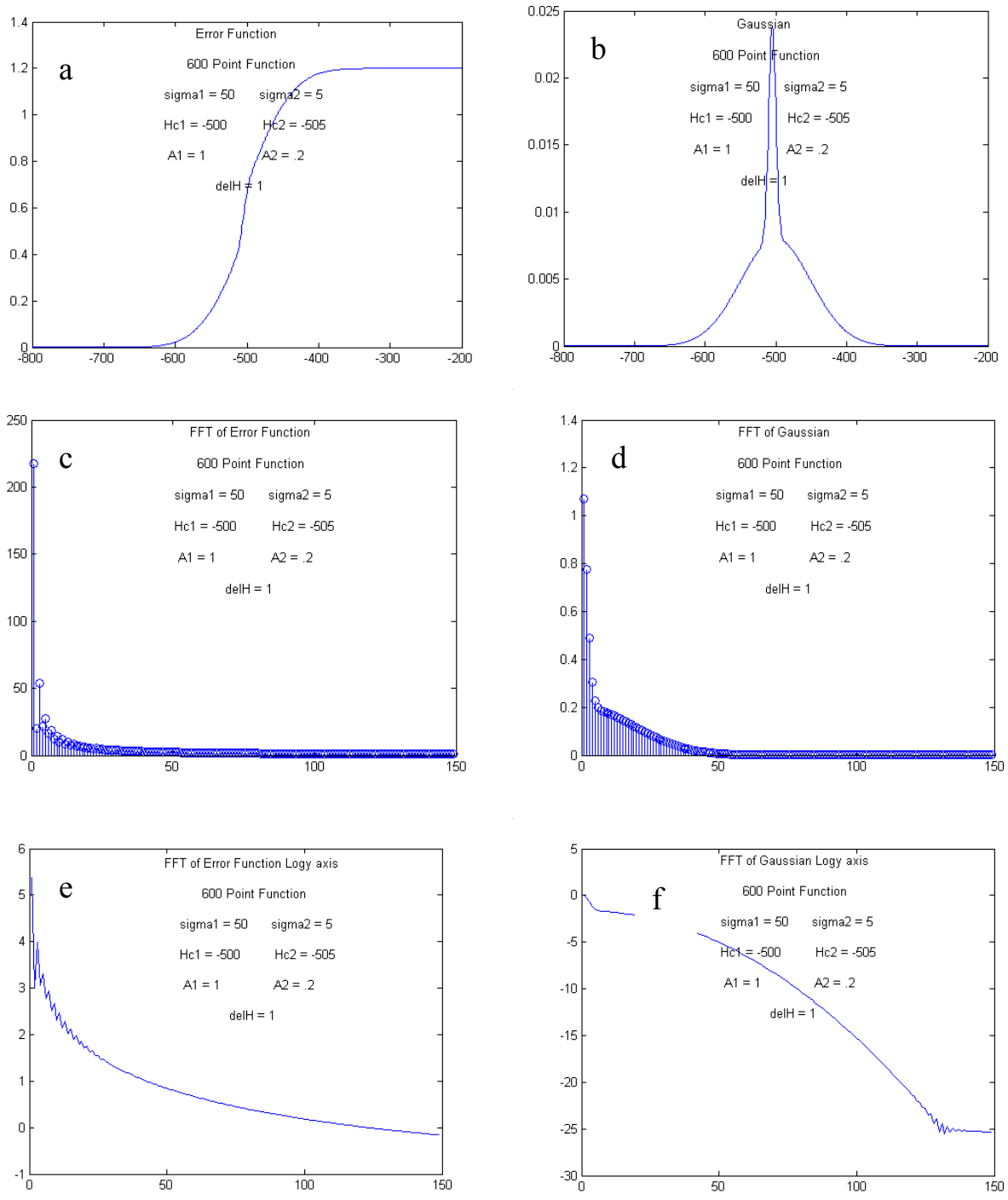

Fig 5.7 Sensitivity of FFT to magnetic markers. FFT of the composite material; Effect of varying the coercivity (mean value of distribution) of the marker on the FFT; Amount Phase 1 = 83%, Phase 2 = 17%. (a) – the *erf* of the matrix; (b) – Gaussian function; (c) – FFT of *erf*; (d) – FFT of Gaussian function; (e) – FFT of erf, magnitude in log axis; (f) – FFT of Gaussian in log axis. σ_1 =50 H_{c1} = -500 Oe A1=1, σ_2 =5 H_{c2} = -505 Oe A2=0.2.

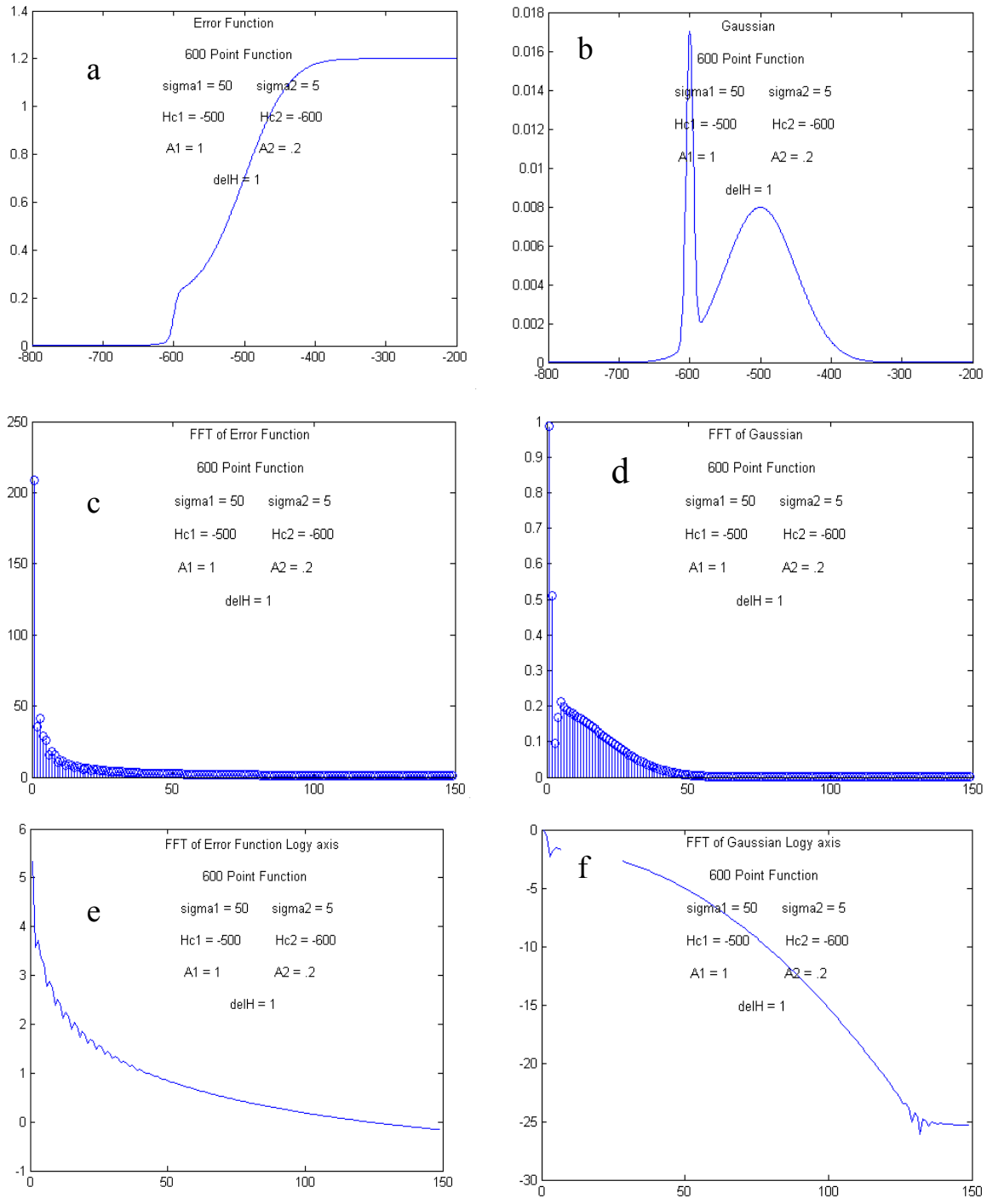

Fig 5.8 Sensitivity of FFT to magnetic markers. FFT of the composite material; Effect of varying the coercivity (mean value of distribution) of the marker on the FFT; amount Phase 1 = 83%, Phase 2 = 17%. (a) – the *erf* of the matrix; (b) – Gaussian function; (c) – FFT of *erf*; (d) – FFT of Gaussian function; (e) – FFT of erf, magnitude in log axis; (f) – FFT of Gaussian in log axis ; σ_1 =50 H_{c1} = -500 Oe A1=1, σ_2 =5 H_{c2} = -600 Oe A2=0.2

6. APPLICATION OF FFT TO MEASURED HYSTERESIS LOOPS

The numerical modeling of the FFT was performed using a simple approximation to the RHL and the SFD, in the form of an error function and a Gaussian distribution. These functions may not exactly represent the hysteresis loop, however it is still a good approximation to assess the effects of various parameters on the FFT. Hence the results of the above sections can be applied to hysteresis loops, measured on actual control materials. The actually measured DHL were fitted to nonlinear functions by TABLECURVE, and the erf, i.e. Gauss cumulative always has a $r^2 \geq 0.98$. The exponentially modified *erf* is a slightly better approximation, and it could be used in the numerical experiments, however, the results, using *erf*, satisfactorily represent the investigated phenomena..

All the measurements were performed using a Vibrating Sample Magnetometer (VSM) on GWU Northern Virginia Campus' s Magnetic Laboratory, established by the P.I. The software of the VSM (Made by *DMS*) includes a variety of built-in hysteresis measurements. The measurement of the major hysteresis loop and the DC remanence loop is a standard feature of the VSM. Mostly typical commercial magnetic materials were used for the test.

Based on the results of the numerical simulation, a strict measurement protocol was set up and followed. The maximum applied field was set at H_{max} = 6000 Oe, well above the saturation field, H_{sat}, of all the measured samples. The magnetic field step was *deltaH* = 5 Oe; and MATLAB's FFT was used. As the mass/volume of the samples is not known, the magnitude of the VSM signal might differ for the members of the pairs of samples. The following experiments were performed:

1. Two identical samples were tested to see if there are any differences due to the measurement and evaluation procedure applied;
2. Two similar samples were measured, originating supposedly from the same manufacturer, but at different times, where subtle changes were expected;
3. Three samples taken from the technological process of preparing Fe-ZnO magnetic nanocomposites were chosen in order to see the effect of large differences on the FFT.

6.1. DELTACARD

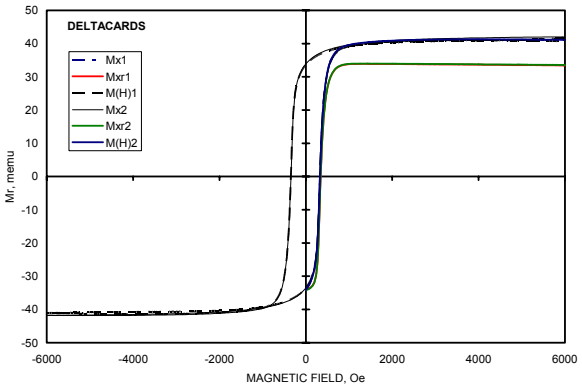

Fig. 6.1. Measured major and DC remanent hysteresis loops for two DELTACARD samples.

Two circular samples of 5mm diameter were cut from the same frequent flyer card ("Deltacard"). The DC remanent loop (RHL) was measured on the VSM for both. The SFD was obtained by numerical differentiation of the $M_r(H)$ curves. Numerical differentiation is very sensitive to measurement errors. Although the magnetization of the cards is not extremely low, the amount of the sample is very small, such that a sensitive range (10^{-3} emu) of the VSM had to be used.

The measured major and remanent hysteresis loops are shown in Fig.6.1 for both DELTACARD samples.

Figs. 6.2 and 6.3 show the measured RHL, the calculated SFD, and the FFT applied to both curves, represented both in linear and log scale.

As both samples were cut from the same card, it was expected that the two are identical, and any difference in either the magnetic measurements, or in the FFT is due to errors in the procedures. As it can be seen, both the measured data, and both the FFT in Fig 6.2 and Fig 6.3 are seemingly identical. However, closer inspection of numerical data for the Fourier coefficients and phase data show some differences (see Fig. 4.8.). Further experiments are necessary to reveal the if these discrepancies are due to real material differences or due to the limits of the RHL measurements as reflected in FFT accuracy.

6.2. METROCARD

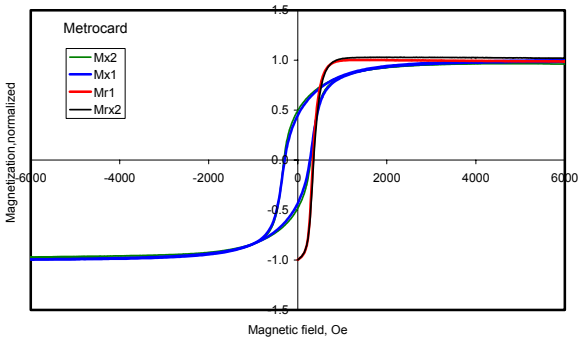

Fig.6.4. Normalized major and DC remanent hysteresis loop measurement data for two METROCARD samples

In this experiment, samples were cut from two different Washington DC subway farecards (METROCARD). It is assumed, that the material comes from the same manufacturer, and the properties of the samples are very close. They might have been made at different times, and there might be some subtle changes.

The measured major and remanent hysteresis loops are shown in Fig. 6.4. The measured magnetization values are normalized to the saturation magnetization to see the subtle differences in the behavior of the two nearly identical samples. Figures 6.5 and 6.6 show the FFTs of two different metro cards. The 2 figures have FFTs similar in nature but different in magnitude, due to the different value of the magnetization of the two samples. When the FFT is performed over data, normalized to the M_{r0} value, they become identical, proving that the manufacturing of the Washington DC subway farecards is a consistent process, based on the same raw materials and same technology, - at least for those farecards, purchased during the second half of November 2002.

6.3. Fe-Zn nanocomposites

Figures 6.7 and 6.8 show the evaluation of measured data for Fe-ZnO magnetic nanocomposites, prepared by mechanochemistry (Courtesy of *Physics Dept, UMBC, Prof. L. Takacs*). The nanocomposites were prepared by reaction milling, according to the following reaction: $Fe_3O_4 + 4\ Zn = 3\ Fe + 4ZnO$. Starting from the relatively large size, magnetically semihard magnetite particles, the end product is nanosize pure Fe particles, embedded in an insulating, nonmagnetic ZnO matrix. The coercivity of the Fe particles depends very sensitively on the microstructure, size, shape, stress state, and interaction effects in the system. According to X-ray, Mössbauer and STEM data, during the actual chemical reaction process there are several intermediate phases present, and the size distribution of the Fe particles is continuously changing during the milling process [2].

This system seems ideal for investigating its properties through FFT, and establish the correlation between the change of the characteristics of the FFT spectrum (amplitude and phase) and results, obtained by traditional methods. Figures 6.7 and 6.8. illustrate the magnetite-zinc system, showing the measured RHL and numerical derivatives, i.e. the SFD curves, together with their corresponding FFT spectra. Fig.6.7 is for a sample at the beginning of the ball milling (20 min), when the magnetic phase consists mostly of the semihard magnetite phase. Fig 6.8. illustrates the nanocomposite after 300 min of milling, when most of the iron is already in the single domain range, with an increased coercivity. The original measurements did not follow the protocol, developed in the present work, and the number of data points and the magnetic field limits are different for the two sets of data, thus the comparison can be only qualitative. Moreover, numerical differentiation makes the FFT of the SFD curves very noisy, thus unusable for identification of finer details.

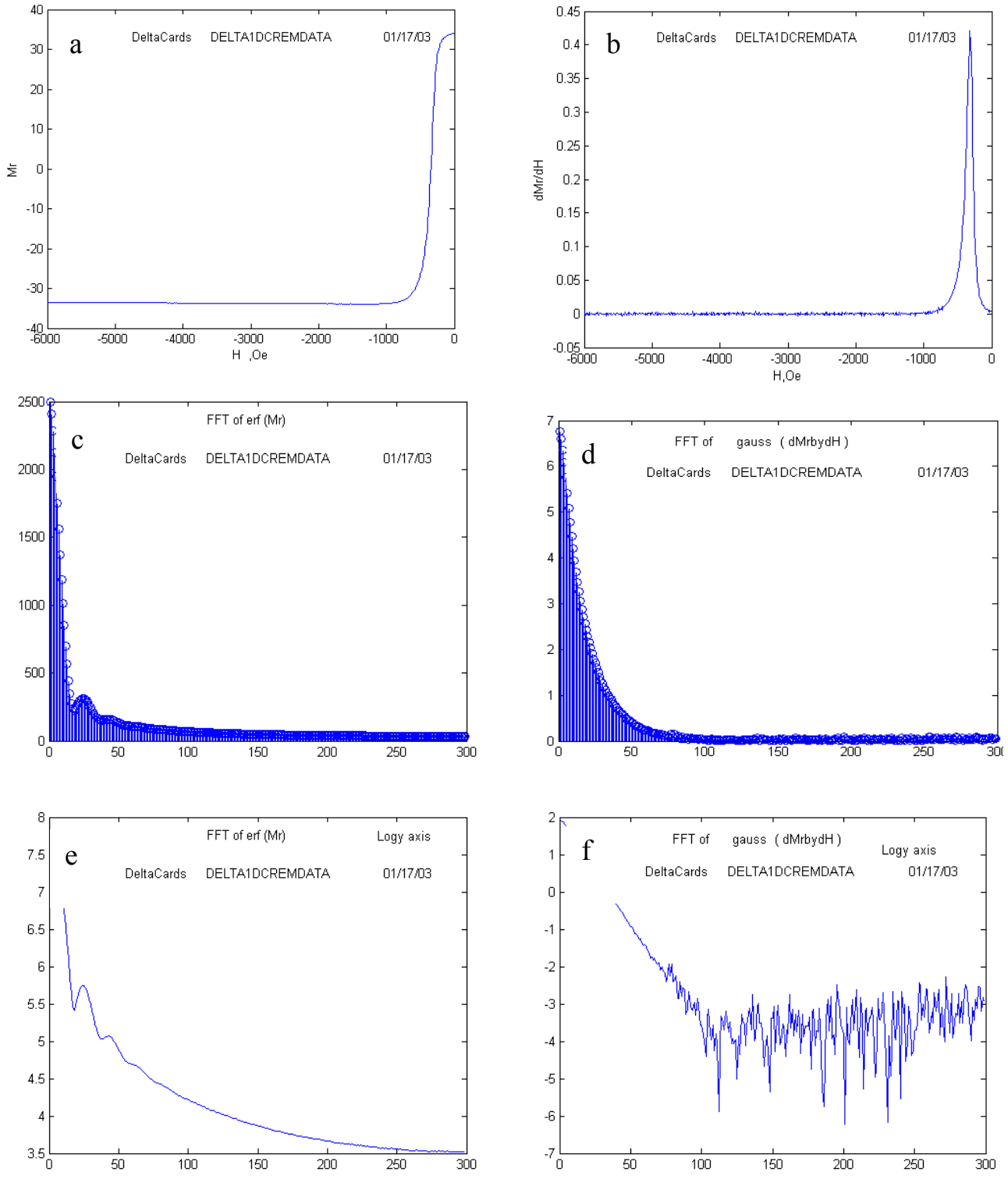

Fig 6.2 Application of FFT to measured hysteresis loops. (a) –RHL for DELTACARD1; (b) - calculated SFD for the RHL; (c) –FFT of RHL; (d) - FFT of the SFD; (e) - FFT of RHL, magnitude in log axis ; (f) FFT of SFD, magnitude in log axis.

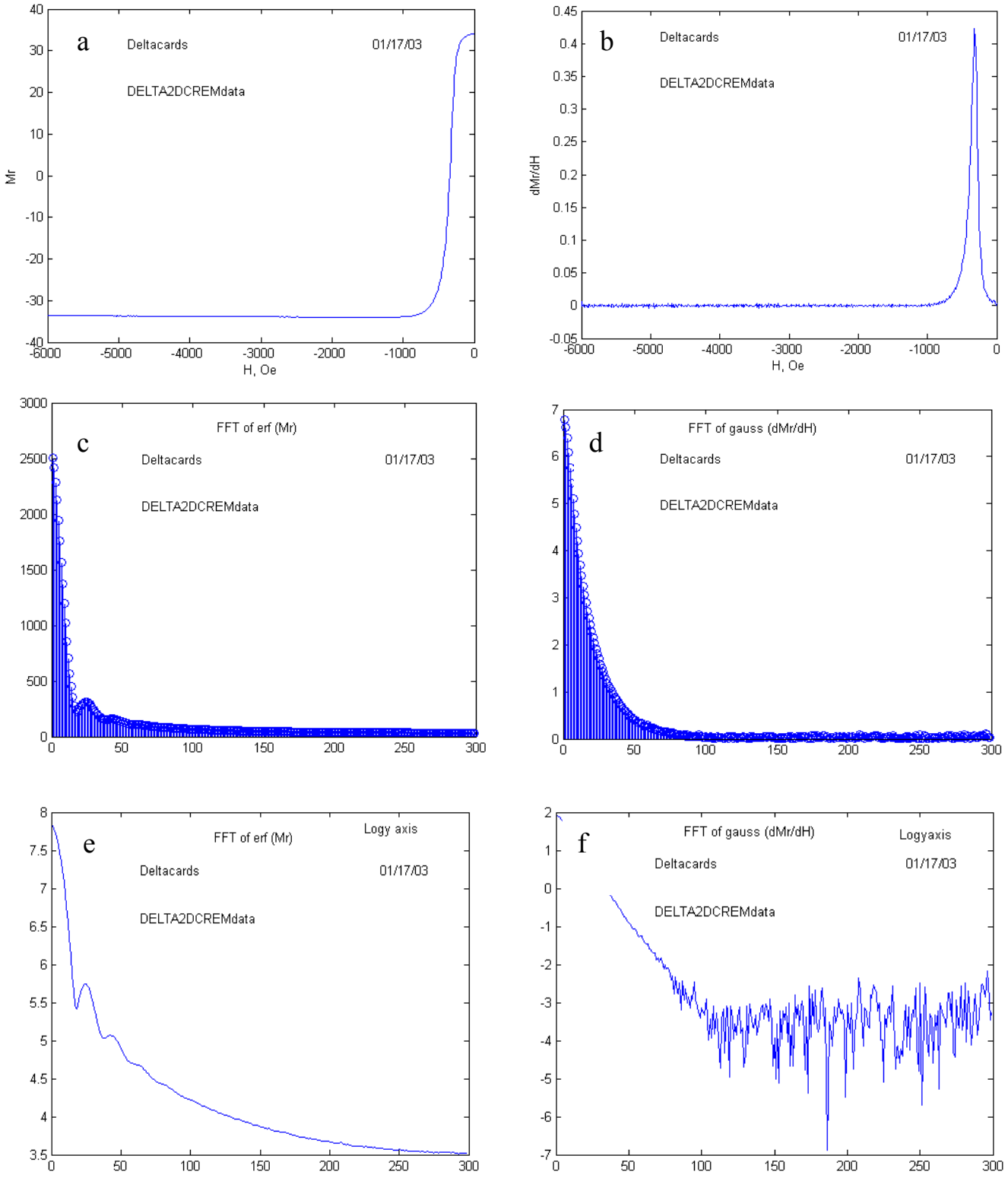

Fig 6. 3. Application of FFT to measured hysteresis loops; (a) –RHL for DELTACARD2; (b)- calculated SFD for the RHL; (c) – FFT of RHL; (d) - FFT of the SFD; (e) - FFT of RHL, magnitude in log axis; (f) FFT of SFD, magnitude in log axis

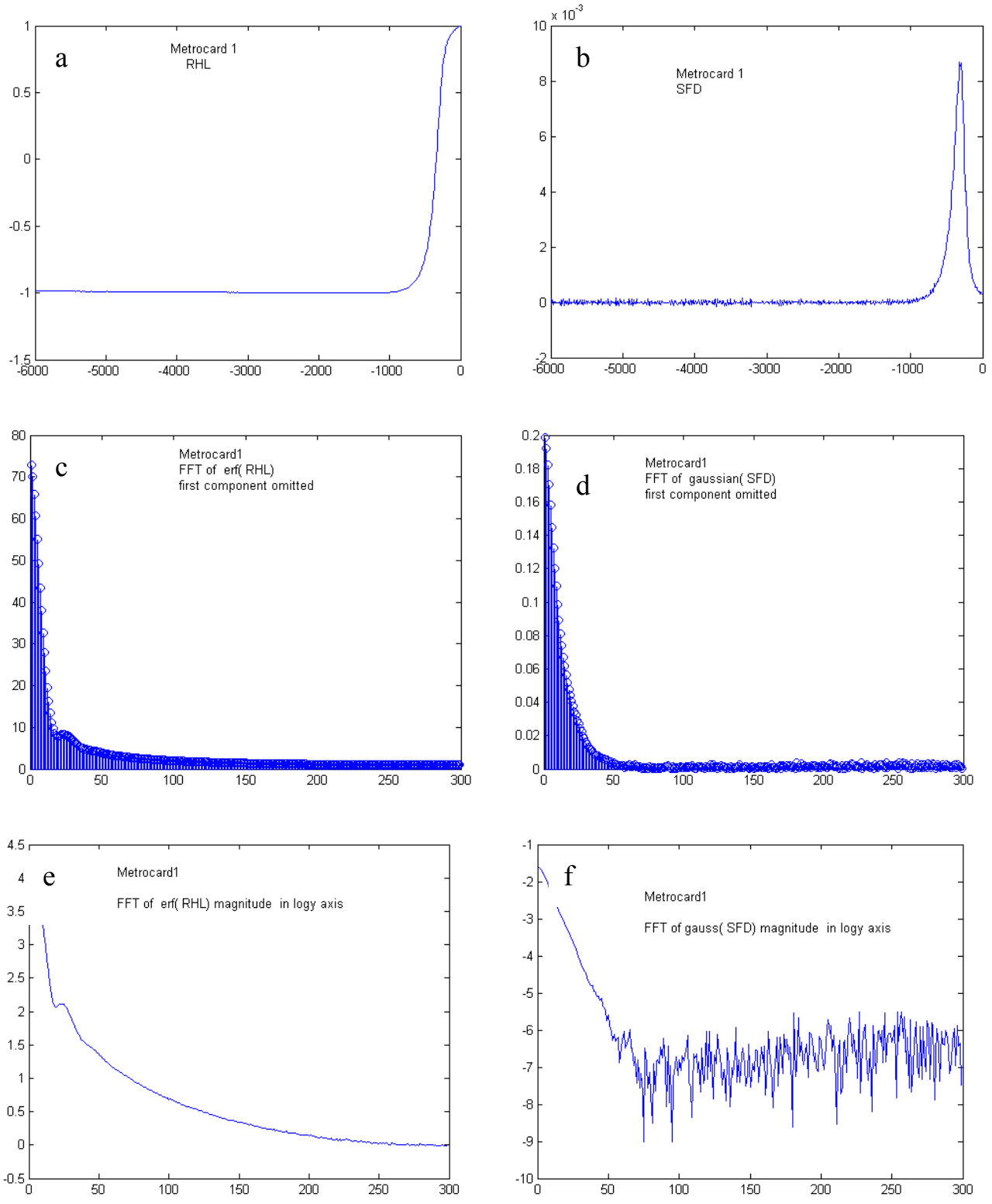

Fig 6.5 Application of FFT to measured hysteresis loops; (a) –RHL for METROCARD1; (b) - calculated SFD for the RHL; (c) – FFT of RHL; (d) - FFT of the SFD; (e) - FFT of RHL, magnitude in log axis; (f) - FFT of SFD, magnitude in log axis

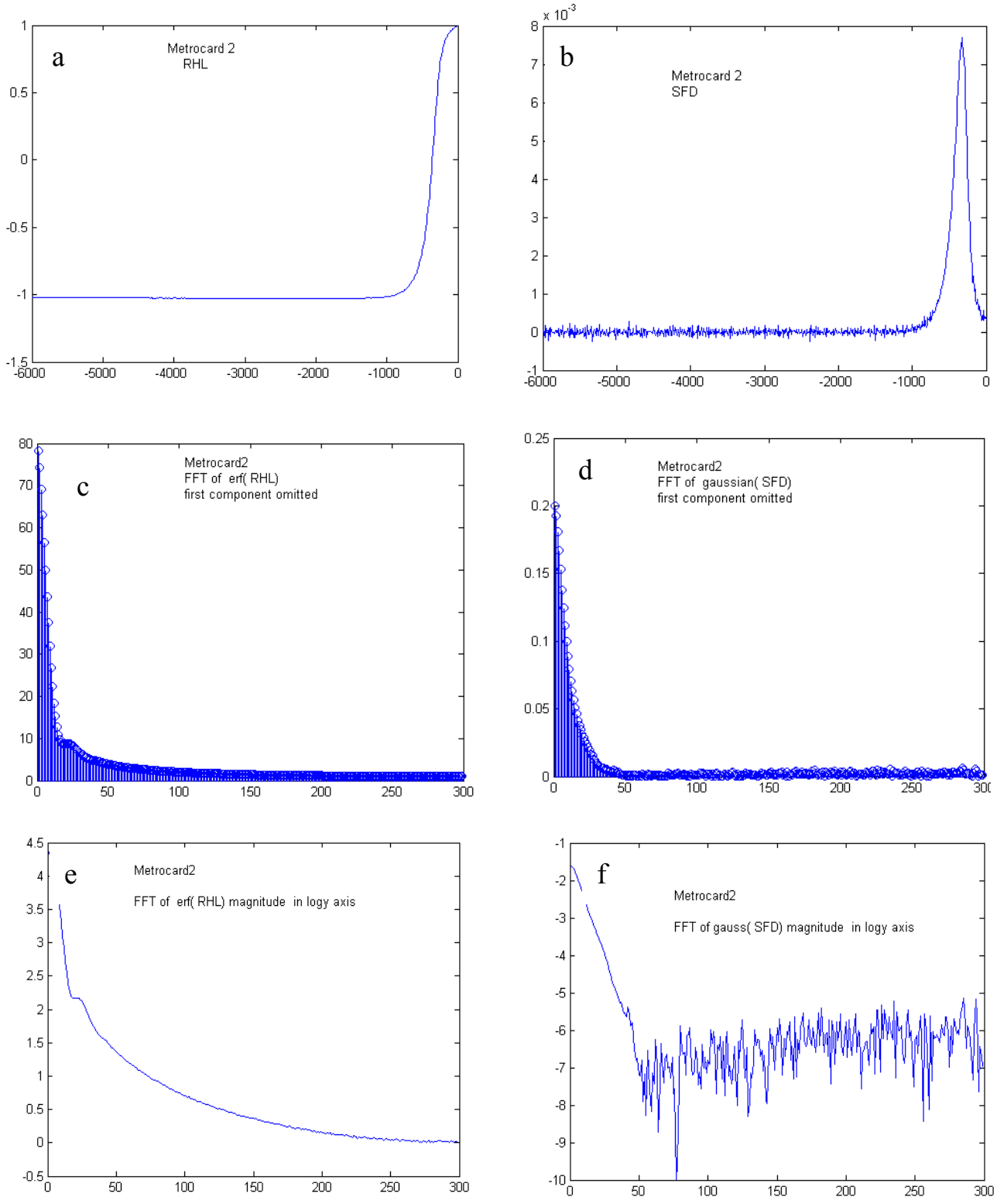

Fig 6.6 Application of FFT to measured hysteresis loops; (a) – RHL for METROCARD2; (b) - calculated SFD for the RHL; (c) – FFT of RHL; (d) - FFT of the SFD; (e) - FFT of RHL, magnitude in log axis; (f) - FFT of SFD, magnitude in log axis

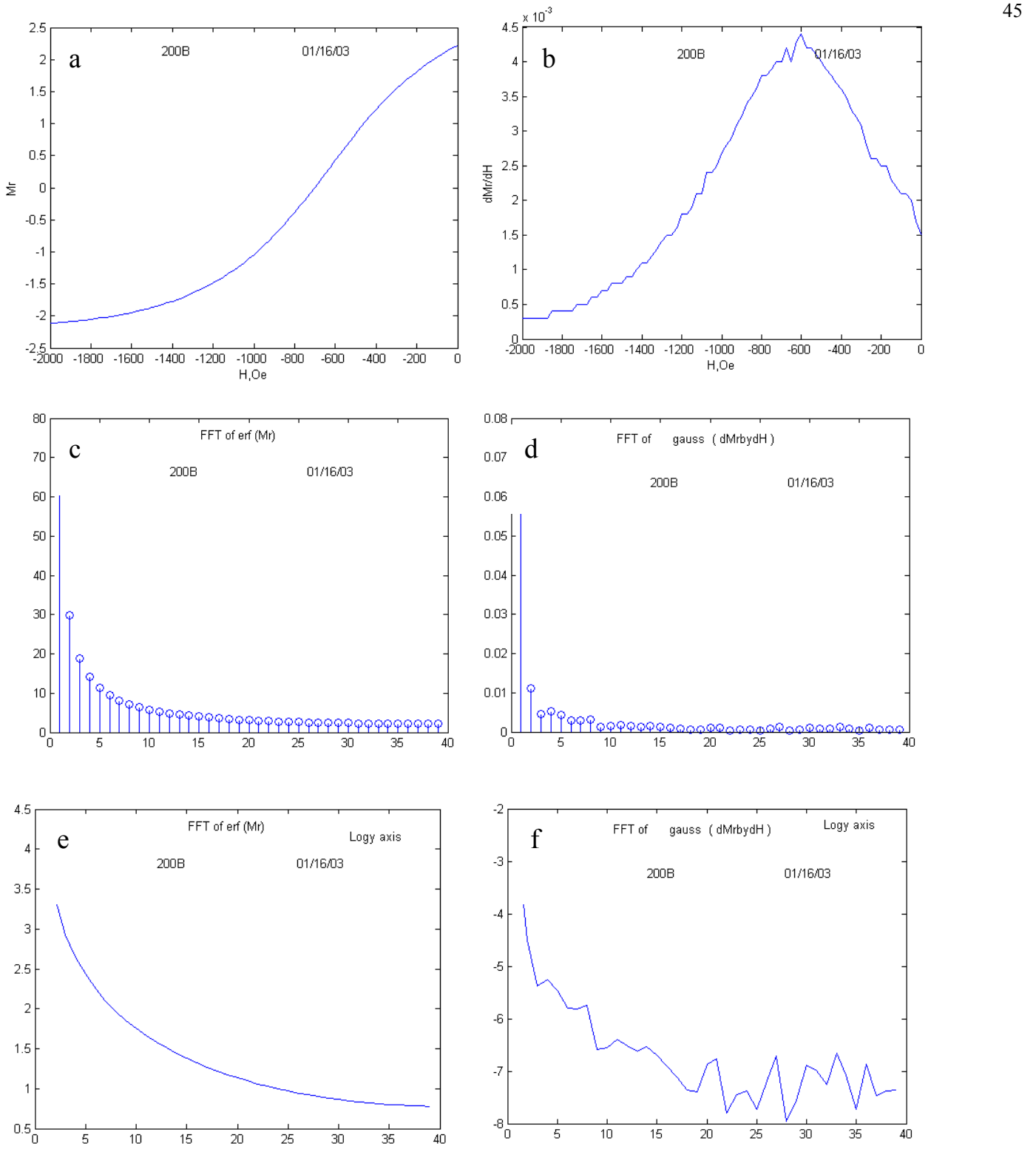

Fig 6.7 Application of FFT to measured hysteresis loops for a series of Fe-ZnO magnetic nanocomposites. (a) –RHL for *FeZn200* (initial mixture); (b) - calculated SFD for the RHL; (c) – FFT of RHL; (d) - FFT of the SFD; (e) -FFT of RHL, magnitude in log axis; f) - FFT of SFD, magnitude in log axis

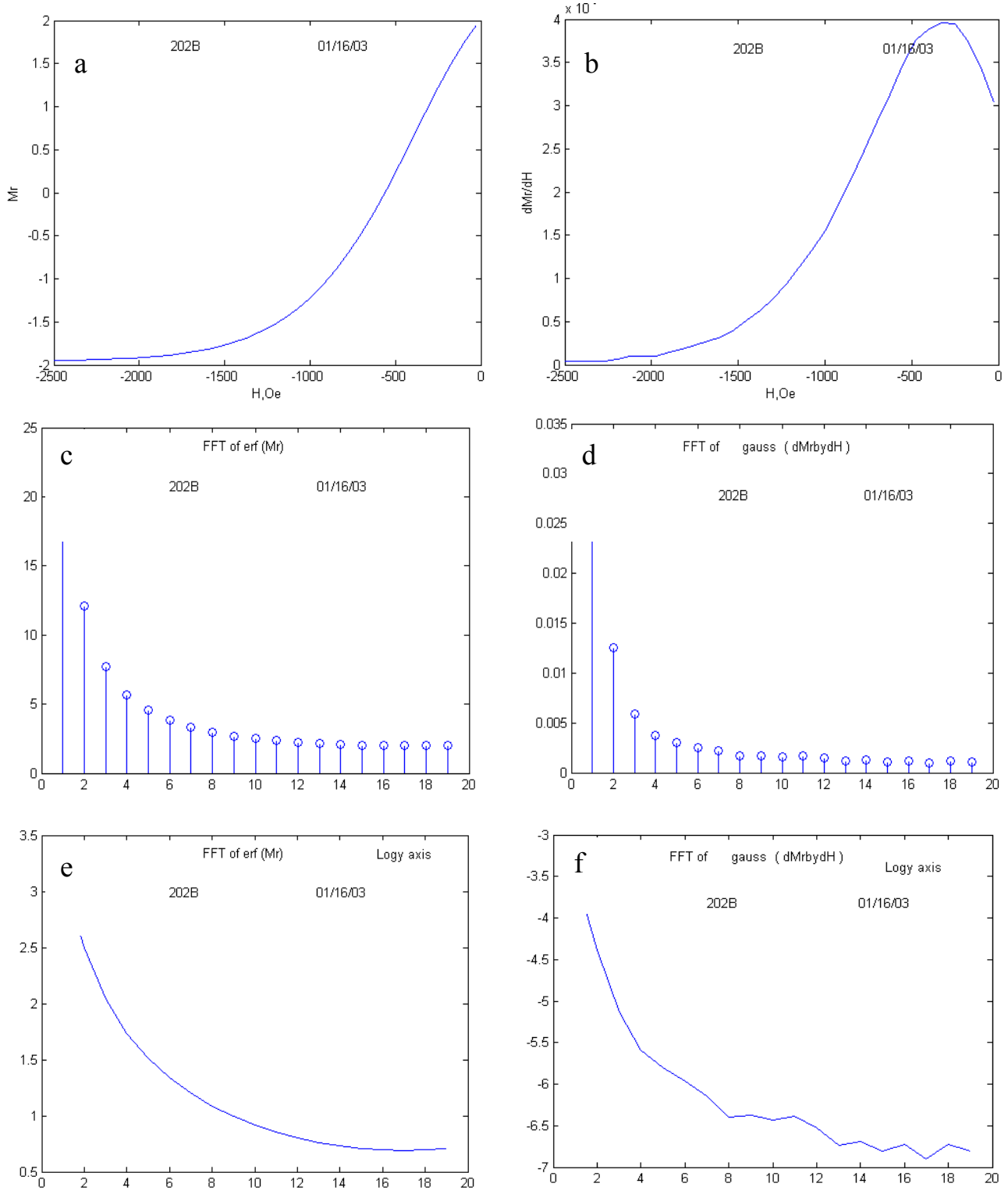

Fig 6.8. Application of FFT to measured hysteresis loops for a series of Fe-ZnO magnetic nanocomposites. (a) –RHL for *FeZn202* (300 min milling); (b) - calculated SFD for the RHL; (c) – FFT of RHL; (d) - FFT of the SFD; (e) - FFT of RHL, magnitude in log axis; (f) - FFT of SFD, magnitude in log axis

7. CONCLUSIONS AND FUTURE RESEARCH DIRECTIONS

The research, performed in the frame of this Project, supported by the U. S. Army Research Office, has shown that applying the FFT to the DC remanent hysteresis loops (RHL) and the switching field distribution (SFD) is a novel approach to magnetic material characterization, connecting technology related microstructural effects, traditional magnetic measurements, and modern signal processing methods to contribute to our basic knowledge about hysteresis with potentially useful applications.

7.1. Summary of main results

The main results of the research are as follow:

- The well-known technique of FFT was used to derive more information from the measured RHL and its derivative, the SFD. In the numerical analysis and simulations the *erf* function is used to represent the RHL and the *Gaussian* function for the SFD.
- Magnetic measurements, as time series, were analyzed in the terms of the Fourier Transform (FT), the Discrete Fourier Transform (DFT), and Fast Fourier Transform (FFT) algorithms. Correspondence between the FT parameters and magnetization, coercivity, saturation field, and magnetic property distribution width was established.
- It was shown analytically that the a_n, b_n coefficients of the FT depend on the width of the switching field distribution through the standard deviation of the Gaussian distribution, both sets depend on the coercivity, represented by δ, and on τ, the time spent in saturation. The field and the coercivity dependence can be separated by using complex Fourier coefficients, where the amplitude depends on τ, and the phase depends on coercivity. The Fourier coefficients strongly depend on the maximum applied field above the saturating field.
- The effects of the model parameters on the FFT of *erf* and Gaussian were numerically simulated, by systematically changing the magnetic parameters of the trial functions and the sampling parameters. Based on the results of the analytical study and the numerical models, a measurement and FFT protocol for analyzing, comparing, and identifying magnetic materials was developed.
- As an application example, the sensitivity of FFT to magnetic markers was investigated numerically, by varying the matrix/marker ratio, and the coercivity of the marker.
- As a practical application, the measurement and FFT protocol, developed in this research, were applied commercial magnetic media (DELTACARD, METROCARD) and Fe-Zn nanocomposites.
- Based on the results, two Abstracts have been submitted to international conferences:
  "*Discrete Fourier Analysis of the Magnetic Hysteresis*" by M. Pardavi-Horvath, S. Morshed, and S. Srinivasan to the 3rd International Conference on Hysteresis and Micromagnetic Modeling HMM2003, to be held in May, 2003, Salamanca, Spain. If accepted, the Proceedings will be published in PHYSICA B.
  "*Fourier Analysis of Magnetic Hysteresis* " by M. Pardavi-Horvath, S. Morshed, and S. Srinivasan, to the International Congress on Magnetism ICM 2003, to be held in July 2003, in Rome, Italy. If accepted, the Proceedings will be published in JMMM.
- There is a significant contribution of the research performed to the education of our students. Two graduate students (one female), and one undergraduate (minority) students were involved in the project. They've got a valuable experience in magnetics, numerical and "real" experiments, data acquisition and evaluation, signal processing, and teamwork, - all combined and applied to one focused topic of the FFT of RHL.

7.2. Proposed further research

This project focused on understanding the underlying physics of the FFT of magnetic hysteresis, using mostly numerical simulation tools. The real proof of the method would be its systematic application to RHL

curves, measured on well-characterized series of real materials. It was shown that the FFT is an important tool in characterizing magnetic materials, if applied with caution and taking into account certain constraints.

One of the open questions is the information, contained in the phase of the complex Fourier coefficients, as one of the most important characteristics, the coercivity, is hidden in the phase of the Fourier components. A study of a series of materials, with systematically varying coercivity, while the magnetization is kept as constant as possible, would be a good test of the phase relationships. It is proposed to investigate a series of Fe-Dielectric Metal Oxide composites where, during the process of mechanochemical preparation, the decrease in size of the pure Fe particles is accompanied by increasing coercivity. VSM, XRD and TEM measurements could serve as control measurements. The P.I. and her colleague (UMBC, Prof Takacs) are pioneers of bulk magnetic nanocomposites, and they have an extensive background in the preparation and control of magnetic properties of reaction milled iron based composites.

Another intriguing problem is the design of a magnetic marker in a *magnetic* material. Numerical simulations, performed in this research, revealed the most important design principles, the phase, coercivity, and amplitude relationships between a magnetic matrix and a magnetic marker. Again, a mixture of magnetic nanocomposites, having controlled coercivities, could serve as a good model material to test the predictions of this project. At the same time, further numerical simulations of the FFT of different (numerical) mixtures of hysteresis loops, measured on “real” materials, could facilitate the design.

LIST OF REFERENCES

[1] M. Pardavi-Horvath and L. Takacs: "Magnetic Nanocomposites by Reaction Milling", Scripta Metallurgica and Materialia, **33**, 1731, 1995.

[2] Martha Pardavi-Horvath, Laszlo Takacs and Ferenc Cser: "Switching field distribution changes during reaction milling of iron-zinc nanocomposites", IEEE Trans. Mag., **31**, 3775, 1995,

[3] M. Pardavi-Horvath: "Characterization of nanostructured magnetic materials", J. Magn. Magn. Mat. **203,** 1-3 pp. 57, 1999.]

[4] E. Della Torre, *Magnetic Hysteresis*, IEEE Press, 1999.

[5] N. Davis, "Derivation and application of an equation to the B-H loop", J. Phys. D: Appl. Phys., **4**, p. 1034, 1971.

[6] S. S. S. N. M. Willcock, "Harmonic Analysis of B-H loops", IEEE Trans. Magn.*;* **MAG-19**, No.5, pp. 2265-2270, 1983.

[7] 7 Udpa and W. Lord: "A Fourier descriptor model of hysteresis loop phenomena", IEEE Trans. Mag., **21**, 2370, 1985.

[8] R. M. Josephs, D. S. Crompton and Ch. S. Krafft: "Characterization of magnetic oxide recording media using Fourier analysis of static hysteresis loops", IEEE Trans. Mag., **22,** 653,1986.

[9] Fedor Gomory: "Use of phase-sensitive detector for measuring magnetic hysteresis loops", Rev. Sci. Instrum., **62**, 2019, 1991.

[10] John L. Wallace: "Real-time fast-Fourier-transform analysis of M-H hysteresis loops", J. Appl. Phys., **73**, 6849, 1993.

[11] V. Masheva, J, Geshev and M. Mikhov: "Fourier analysis of hysteresis loops and initial magnetization curves: application to the singular point detection method", J. Magn. Magn. Mater., **137**, 350,1994.

[12] J. Geshev, V. Masheva, and M. Mikhov, "Interaction Effects Deteced by Fourier Analysis of Hysteresis Loops and Initial Magnetization Curves" IEEE Trans. Magn., **30**, No. 2, pp. 863-865, 1994.

[13] V. Masheva, J. Geshev, and M. Mikhov, "The Influence of the Second Anisotropy Constant on the Fourier description of Hysteresis Loops for a Stoner" JMMM., **140-144,** pp. 371-372, 1995.

[14] N. I Shakshin, G. I. Deordiev, V. E. Scherbinin, V. Moorthy, T. Jayakumar, D. K. Bhattacharya, P. Kalyanasundaram, and B. Raj, "Evaluation of thermal ageing conditions in 17-4 PH stainless steel by Fourier descriptor analysis of magnetic hysteresis loops" ScienceDirect - NDT & E International/ SCIRUS, **29,** Issue 6, pp. 379-385, 1996.

[15] S. Thamm and J. Hesse, "A simple plot indicating interactions between single-domain particles" JMMM, **154**, , pp.254-262, 1996.

[16] A. Mohammed, B. A. R. Al-Hashemy, and M. A. Tawfik, "A Fourier Descriptor Model of Hysteresis Loops for Sinusoidal and Distorted Waveforms" IEEE Trans. Magn.,. **33**, No. 1, pp. 686-691, 1997.

[17] J. Geshev and J.E. Schmidt, "Interaction Fields Evaluation in Fine Particle Systems" IEEE Trans. Magn., **33**, No. 4, pp. 2504-2508, 1997.

[18] Zh.Liu, X.Y.Wei, K.Tsukada, and K.Hanasaki, "Steel property evaluation from the hysteresis loop by using Fourier Descriptors", SICE, pp. 971-976, July 1997

[19] M. Sjostrom, "Frequency Analysis of Classical Preisach Model" IEEE Trans. Magn., **35**, No. 4, pp. 2097-2103, 1999.

[20] Salceanu and V. David, "Programs and virtual hysteresis graph for scalar Preisach modeling" in ScienceDirect - Computer Standards and Interfaces/ SCIRUS, **21**, issue 4, pp. 349-356, 1999.

[21] *MATLAB, ORIGIN, TABLECURVE, FFTPACK at NETLIB;*

[22] J. S. Walker: *Fast Fourier Transforms,* CRC Press, Boca Raton, 1996.

[23] F. Hoffman, *An Introduction to Fourier Theory,* http://utcsl.phys.utk.edu/~forrest/papers/fourier/index.html

[24] http://chsfpc5.chem.ncsu.edu/CH795Z/math/ft/gaussian.html

[25] D. Wagenaar, *Fourier Transform Examples* for JPNM Physics, http://www.med.harvard.edu/JPNM/physics/didactics/improc/intro/fourier3.html

[26] P. Bourke, *DFT (Discrete Fourier Transform) FFT (Fast Fourier Transform),* http://astronomy.swin.edu.au/~pbourke/analysis/dft , 1993.

[27] R. Strum and D. Kirk, *Contemporary Linear Systems Using Matlab*, Brooks/Cole Thomson Learning, pp. 543-614, 1999.

MASTER COPY: PLEASE KEEP THIS "MEMORANDUM OF TRANSMITTAL" BLANK FOR REPRODUCTION PURPOSES. WHEN REPORTS ARE GENERATED UNDER THE ARO SPONSORSHIP, FORWARD A COMPLETED COPY OF THIS FORM WITH EACH REPORT SHIPMENT TO THE ARO. THIS WILL ASSURE PROPER IDENTIFICATION. NOT TO BE USED FOR INTERIM PROGRESS REPORTS; SEE PAGE 2 FOR INTERIM PROGRESS REPORT INSTRUCTIONS.

MEMORANDUM OF TRANSMITTAL

U.S. Army Research Office
ATTN: AMSRL-RO-BI (TR)
P.O. Box 12211
Research Triangle Park, NC 27709-2211

☐ Reprint (Orig + 2 copies)
☐ Technical Report (Orig + 2 copies)
☐ Manuscript (1 copy)
☐ Final Progress Report (Orig + 2 copies)
☐ Related Materials, Abstracts, Theses (1 copy)

CONTRACT/GRANT NUMBER:

REPORT TITLE:

is forwarded for your information.

SUBMITTED FOR PUBLICATION TO (applicable only if report is manuscript):

Sincerely,